DOE/NASA/0352-1
NASA CR-174893
DEN3-352

Sliding Seal Materials For Adiabatic Engines Phase I Interim Report

James Lankford
Southwest Research Institute
San Antonio, Texas

April 1985

Prepared for
NATIONAL AERONAUTICS AND SPACE ADMINISTRATION
Lewis Research Center
Under Contract DEN3-352

for
U.S. DEPARTMENT OF ENERGY
Conservation and Renewable Energy
Office of Vehicle and Engine R&D

DOE/NASA/0352-1
NASA CR-174893
DEN3-352

Sliding Seal Materials For Adiabatic Engines Phase I Interim Report

James Lankford
Southwest Research Institute
San Antonio, Texas

April 1985

Prepared for
National Aeronautics and Space Administration
Lewis Research Center
Cleveland, Ohio 44135
Under Contract DEN3-352

for
U.S. DEPARTMENT OF ENERGY
Conservation and Renewable Energy
Office of Vehicle and Engine R&D
Washington, D.C. 20545
Under Interagency Agreement DE-AI01-80CS50194

1. Report No.	2. Government Accession No.	3. Recipient's Catalog No.
NASA CR-174893		UC-96

4. Title and Subtitle	5. Report Date
Sliding Seal Materials for Adiabatic Engines	April 1985
	6. Performing Organization Code

7. Author(s)	8. Performing Organization Report No.
James Lankford	06-7963
	Feb. 1984-Feb. 1985
	10. Work Unit No.

9. Performing Organization Name and Address	11. Contract or Grant No.
Southwest Research Institute 6220 Culebra Road, P.O. Drawer 28510 San Antonio, Texas 78284	DEN3-352
	13. Type of Report and Period Covered
12. Sponsoring Agency Name and Address	Interim Contractor Report
U.S. Department of Energy Office of Vehicle and Engine R&D Washington, D.C. 20545	14. Sponsoring Agency Code DOE/NASA/0352-1

15. Supplementary Notes

Phase I Interim Report. Prepared under Interagency Agreement DE-AI01-80CS-50194. Project Manager, Howard G. Yacobucci, Propulsion Systems Division, NASA Lewis Research Center, Cleveland, Ohio 44135.

16. Abstract

An essential task in the development of the heavy-duty adiabatic diesel engine is identification and improvements of reliable, low-friction piston seal materials. In the present study, the sliding friction coefficients and wear rates of promising carbide, oxide, and nitride materials were measured under temperature, environmental, velocity, and loading conditions that are representative of the adiabatic engine environment.

In order to provide guidance needed to improve materials for this application, the program stressed fundamental understanding of the mechanisms involved in friction and wear. Microhardness tests were performed on the candidate materials at elevated temperatures, and in atmospheres relevant to the piston seal application, and optical and electron microscopy were used to elucidate the micromechanisms of wear following wear testing. X-ray spectroscopy was used to evaluate interface/environment interactions which seemed to be important in the friction and wear process.

Electrical effects in the friction and wear processes were explored in order to evaluate the potential usefulness of such effects in modifying the friction and wear rates in service. However, this factor was found to be of negligible significance in controlling friction and wear.

17. Key Words (Suggested by Author(s))	18. Distribution Statement
Ceramics; friction; wear; temperature effects; environmental effects	Unclassified-Unlimited STAR 27,85 DOE Cat. UC-96

19. Security Classif. (of this report)	20. Security Classif. (of this page)	21. No. of Pages	22. Price*
Unclassified	Unclassified	61 + Prelim.	

* For sale by the National Technical Information Service, Springfield, Virginia 22161

NASA-C-168 (Rev. 10-75)

ABSTRACT

An essential task in the development of the heavy-duty adiabatic diesel engine is identification and improvement of reliable, low-friction piston seal materials. In the present study, the sliding friction coefficients and wear rates of promising carbide, oxide, and nitride materials were measured under temperature, environmental, velocity, and loading conditions that are representative of the adiabatic engine environment.

In order to provide guidance needed to improve materials for this application, the program stressed fundamental understanding of the mechanisms involved in friction and wear. Microhardness tests were performed on the candidate materials at elevated temperatures, and in atmospheres relevant to the piston seal application, and optical and electron microscopy were used to elucidate the micromechanisms of wear following wear testing. X-ray spectroscopy was used to evaluate interface/environment interactions which seemed to be important in the friction and wear process.

Electrical effects in the friction and wear processes were explored in order to evaluate the potential usefulness of such effects in modifying the friction and wear rates in service. However, this factor was found to be of negligible significance in controlling friction and wear.

TABLE OF CONTENTS

		Page
I.	INTRODUCTION	1
	A. Background	1
	B. Required Properties of Seal Materials	3
	C. Wear Behavior of Ceramics	3
	D. Potential Seal Materials	6
	E. Electrical Effects on Hardness and Wear of Carbides	7
II.	EXPERIMENTAL APPROACH	8
	A. Background	8
	B. Materials	8
	C. Wear Testing	9
	D. Microhardness Tests	9
	E. Wear Characterization	13
III.	RESULTS	14
	A. Indentation Tests	14
	1. Hardness	14
	2. Fracture Toughness	14
	B. Wear Tests	27
	1. Friction Coefficients	27
	2. Wear Rates	27
	3. Wear Characterization	41
IV.	DISCUSSION	57
V.	CONCLUSIONS	59
VI.	REFERENCES	60

LIST OF ILLUSTRATIONS

Table		Page
I	Material Properties	10
II	Friction and Wear Test Parameters	12

Figure		
1	Crosshead Engine Schematic	2
2	Schematic of Engine with Full-Length Ceramic Cylinder Liner	4
3	Sketch of High-Temperature Friction and Wear Test Apparatus	11
4	Hardness Versus Temperature for NC 132 in DE and Ar	15
5	Hardness Versus Temperature for PSZ in DE and Ar	16
6	Hardness Versus Temperature for NiMo-TiC in DE and Ar	17
7	Hardness Versus Temperature for SiC in DE and Ar	18
8	Hardness Versus Temperature for TiC in DE and Ar	19
9	Hardness Versus Temperature for All Materials in DE	20
10	Hardness Versus Applied Electrical Potential for SiC at 23°C in Humid Air	21
11	Fracture Toughness Versus Temperature for NC 132 in DE and Ar	22
12	Fracture Toughness Versus Temperature for SiC in DE and Ar	23
13	Fracture Toughness Versus Temperature for TiC in DE and Ar	24
14	Fracture Toughness Versus Temperature for NC 132, SiC, and TiC in DE	25
15	Fracture Toughness Versus Applied Electrical Potential for SiC at 23°C in Humid Air	26
16	Friction Coefficient Versus Temperature for K162B Pins/PSZ Disk in DE and Ar	28

LIST OF ILLUSTRATIONS (CONTINUED)

Figure		Page
17	Friction Coefficien Versus Temperature for SiC Pins/PSZ Disk in DE and Ar	29
18	Friction Coefficient Versus Temperature for TiC Pins/PSZ Disk in DE and Ar	30
19	Friction Coefficient Versus Temperature for K162B Pins/NC 132 Disk in DE and Ar	31
20	Friction Coefficient Versus Temperature for SiC Pins/NC 132 Disk in DE and Ar	32
21	Friction Coefficient Versus Temperature for TiC Pins/NC 132 Disk in DE and Ar	33
22	Friction Coefficient Versus Temperature for All Pin Materials on PSZ Disks in Ar	34
23	Friction Coefficient Versus Temperature for All Pin Materials on NC 132 Disks in Ar	35
24	Friction Coefficient Versus Temperature for All Pin Materials on PSZ Disks in DE	36
25	Friction Coefficient Versus Temperature for All Pin Materials on NC 132 Disks in DE	37
26	Wear Rate Versus Temperature for PSZ Disks in Ar	38
27	Wear Rate Versus Temperature for PSZ Disks in DE	39
28	Wear Rate Versus Temperature for NC 132 Disks in DE and Ar	40
29	SiC Pin/NC 132 Disk, 23°C in DE	42
30	Examples of Delamination in NC 132 and PSZ Disks During Equilibrium Stage of Wear, 23°C in DE	43
31	Delamination Development in PSZ Disks During Sliding of SiC Pins at 23°C in DE	44
32	PSZ Delaminate Sheets Lying on the Surface of the PSZ Disk	45
33	PSZ Deposited onto SiC Pins at 23°C in DE	46

LIST OF ILLUSTRATIONS (CONTINUED)

Figure		Page
34	Transfer of PSZ Disk Material to, and Plastic Deformation of, SiC Pin Material	47
35	SiC Pin Wear Due to Plastic Deformation Induced by a PSZ Disk, 23°C, DE	48
36	Wear of K162 Pins/NC 132 Disk in DE at 23°C	49
37	Wear of K162B Pins/NC 132 Disk in Ar at 23°C	51
38	TiO_2 Deposits on NC 132 Disks Run Against TiC Pins in DE	52
39	K162B Pin, After Wear Test Against NC 132 Disk at 800°C in Ar	53
40	NC 132 Wear Track, After Wear Test Against K162B Pins at 800°C in Ar	54
41	K162 Pin/NC 132 Disk Wear Surfaces After Testing at 800°C in DE	55

I. INTRODUCTION

A. Background

Since ten to thirty percent of the work output of an internal combustion engine is expended on the cooling system (1), there is great interest in developing an uncooled diesel engine. Nearly adiabatic operation and recovery of exhaust heat in a turbocompounding system could increase the thermal efficiency of such an engine to 48% (2). Additional benefits could be multifuel capability, reduced noise, reduced white smoke emissions, lower compression ratio, and reduced maintenance (2). The engine would be lighter and easier to produce because of the elimination of the need for a cooling jacket. A recent study by Teledyne Continental Motors for NASA-Lewis Research Center projected important benefits of the use of lightweight adiabatic diesel engines in general aviation aircraft (3,4). The study determined that use of cylinder liners and piston caps of ceramic could save 18% in fuel consumption over current technology.

In the last decade there have been several small-scale demonstrations that ceramic components could perform successfully, in small laboratory diesel engines (1,2,5), and in the last few years ambitious programs have been undertaken to demonstrate the commercial feasibility of adiabatic diesel engines utilizing ceramic parts. In the U.S.A., the largest effort has been the Cummins Engine Company program supported by the U.S. Army Tank Automotive Research and Development Command (TARADCOM), which is developing a six-cylinder diesel of about 500 hp for use in trucks. The design incorporates an insulating ceramic piston cap, cylinder head "hot plate", deck spacer, exhaust ports, manifold, valves, and injectors of insulating ceramic. One experimental engine built utilized hot-pressed silicon nitride, one used zirconia, and another used lithium-aluminum-silicate glass ceramics (2). An interesting approach explored by this program was the use of plasma-sprayed zirconia as a piston crown coating for thermal insulation. Although spalling due to thermal expansion mismatch sets an upper limit on coating thickness, coated pistons have been successfully demonstrated in a laboratory engine. Progress in the program has been outstanding, and expenditures to develop the adiabatic engine are projected to exceed $20,000,000 in the period 1982-1986.

Meanwhile, other countries are also competing to develop the adiabatic engine. In particular, the Ministry of International Trade and Industry of Japan recently launched a ten-year, $60,000,000 project to improve high-technology ceramics, largely for heat engine applications. NGK Spark Plug has reported successful operation of an "all-ceramic" (silicon nitride) diesel engine, which achieved a 30% fuel consumption reduction because the cooling system was eliminated. Kyoto Ceramics, in cooperation with Isuzu Motors, has demonstrated a radiatorless, ceramic diesel engine in an automobile; the silicon nitride piston reportedly experienced temperatures of up to 1200°C without failure.

In comparison to the overall effort on ceramic diesel engine development, little work has been done in the important area of developing a ceramic seal system capable of performing adequately under these harsh conditions.

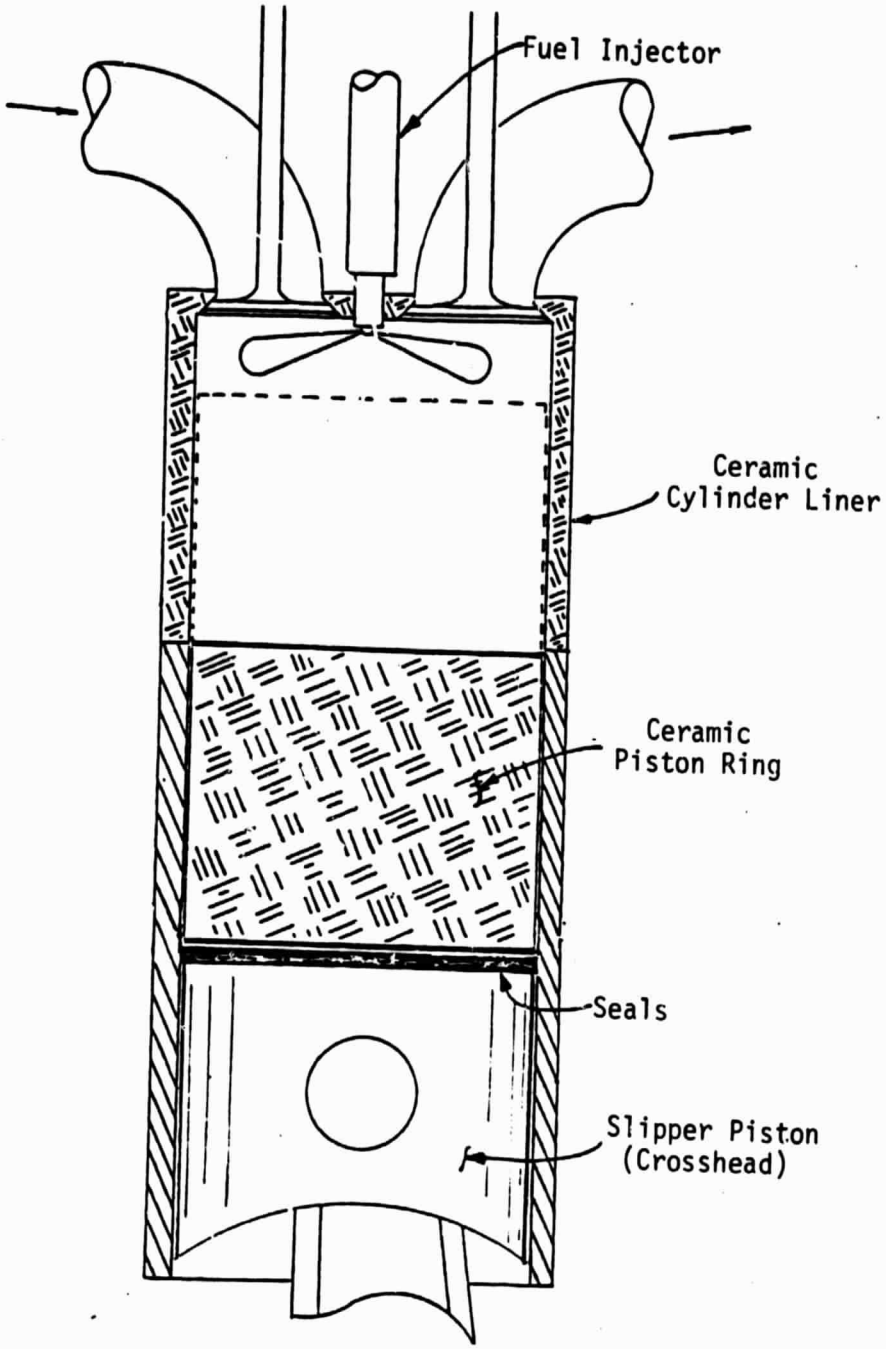

Figure 1. Crosshead Engine Schematic. Seals on the metal crosshead slide on metal cylinder wall.

This report outlines the results of the first year of an ongoing research program which is providing friction and wear data on promising ceramic materials for piston rings in the adiabatic diesel engine, and which is producing basic understanding of the wear processes operative under these conditions.

B. Required Properties of Seal Materials

As outlined above, there has been considerable progress in development of ceramic pistons (or piston caps) and cylinder liners for adiabatic diesel engines. Designs which involve a piston cap in a crosshead engine (Figure 1) can use conventional chromium-plated cast iron rings and low-temperature lubrication, which offers a very low friction coefficient (about 0.05) and low wear rates. However, in a radiatorless engine, the temperature of the metal is likely to become unacceptably hot. Also, this type of design is bulky, involving extra piston weight and high inertial forces on the connecting rod and on the joint between the piston and the ceramic piston cap. On the other hand, a simpler design in which the entire cylinder is ceramic-lined (Figure 2) requires that the piston ring slide against the ceramic liner, which will be quite hot. For this purpose, there is an urgent need to find materials from which sliding seal rings can be made which will exhibit low friction and low ring and liner wear while sliding against a ceramic cylinder liner at high velocity and high temperature.

The piston crown temperature must be raised to at least 882°C in order to achieve significant energy savings in the adiabatic diesel (6); Kyoto Ceramics has operated an engine with peak crown temperatures of 1200°C, and there is interest in pushing the temperature to 1500°C with zirconia engine parts. Thus the prime requirement of the cylinder liner/seal ring system is resistance to thermal shock and retention of strength to temperatures much higher than that which the top ring in a conventional diesel may experience. The liner/ring combination must exhibit acceptable wear rates not only at high temperature, but also at high velocities of as much as 5-10 m/s, and under conditions of exposure to combustion products and excess oxygen. Low friction is essential. The liner materials of interest have been silicon carbide, silicon nitride, and partially-stabilized zirconia. The silicon carbide, although it has been used for solid lifters and precombustion chambers in the heavy-duty diesel program, has a high thermal conductivity, which reduces its usefulness for piston crown and cylinder liner applications. Silicon nitride has been the material of choice in most of the recent work, because of its low thermal conductivity, relatively high strength at temperatures to about 1100°C, resistance to thermal shock, and relative ease of manufacture in complex shapes. However, in the push for higher temperatures still, the limits of silicon nitride are already being approached, and there is interest in zirconia, which is strong even at 1500°C and has better insulating properties than silicon nitride.

C. Wear Behavior of Ceramics

Ceramic systems exhibit a number of wear mechanisms. Adhesion, which is a common cause of wear in metal systems, can also occur between nonmetallic materials, even at low temperature, if clean surfaces of suitably

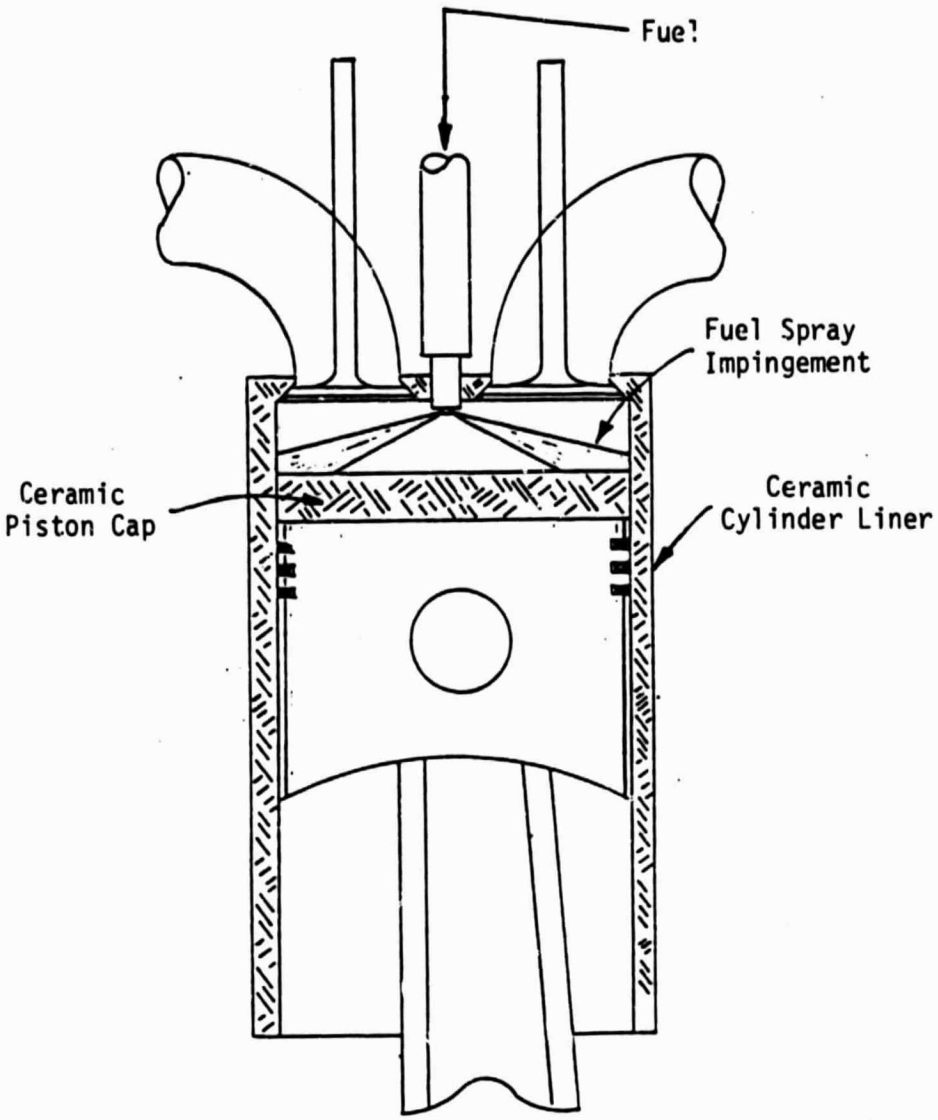

Figure 2. Schematic of Engine with Full-Length Ceramic Cylinder Liner. Piston cap does not have to be as long as the stroke, but the seals now slide on hot ceramic liner.

oriented crystals come into contact. However, due to adsorption and lubrication effects, adhesive wear is not a common problem in ceramic/ceramic sliding couples (7), although it can be a problem with metal/ceramic couples. When metal rubs against ceramic the metal frequently adheres to the ceramic surface (especially if the metal is chemically active, or has a large percentage of d character in its bonding (8,9)). The friction and wear phenomena may then become more a matter of the metal sliding against itself than of metal/ceramic sliding, and the friction often becomes quite high. Ductile plowing is another mode of wear which is common in metals, but which occurs only rarely in ceramic/ceramic systems. A more common wear mode in ceramics seems to be cracking (abrasive wear), which can take many forms (10): cleavage of individual grains, intergranular cracking, lateral cracking or chipping, etc.

Recently, progress has been made in modeling certain types of abrasive wear. It has been established, for example, that for indentation by a sharp indenter, the critical load for subsurface lateral (parallel to the surface) microfracture is given by (11)

$$P_c = A_1 \left(\frac{K_c}{H}\right)^3 K_c$$

where A_1 is a geometric constant, K_c is the fracture toughness, and H is the hardness. Now, if the indenter were to slide over the surface, and if the normal loading P were to exceed P_c, one would anticipate that within the plastic wake of the indenter, a family of lateral cracks would be produced. The removal of these flakes of material following the initial or subsequent passes would then constitute the principal wear mechanism.

Analysis (12) indicates that during the sliding of a sharp indenter, the size of lateral cracks in the wake will be on the order of

$$C = A_2 \left[\frac{(E/E)^{3/5}}{K_c^{1/2} H^{1/8}}\right] f(P, \mu)$$

where A_2 is a constant, E is the elastic modulus, and μ is the friction coefficient. The associated volume removed is then

$$V = A_3 \left[\frac{(E/H)^{4/5}}{K_c^{1/2} H^{5/9}}\right] f(P, \mu) L$$

where A_3 is a constant, and L is the distance slid by the indenter.

It has been observed that when a sharp diamond indenter slides across aluminum oxide (13), wear proceeds by lateral cracking, as predicted in the above analysis. Similarly, sliding of a hemispherical diamond over silicon carbide produces circular ring cracks whose interaction and intersection to produce wear particles has been observed (10) and predicted (14). However, sliding and wear of macroscopic surfaces, neither of which is as hard as diamond, presents a more complicated situation than the idealized cases

cited above. That is, the particular relationship between V and E, H, K_C, H, and μ outlined above may not hold. Nevertheless, it seems reasonable to believe, based on these analyses, that K_C and H in particular should be significant controlling factors in abrasive ceramic/ceramic wear under many circumstances.

The chemical environment also plays a critical role in the wear performance of ceramic materials (10). Adsorbed water promotes near-surface plasticity leading to a soft surface layer some 1-10 micrometers thick. This soft surface layer seems to prevent adhesion and to lubricate ceramics as they slide over each other, so that the friction coefficient (μ) is often only about 0.2 (7). In alumina, for instance, the coefficient of friction rose from 0.25 to 0.8 as the temperature of the experiment was raised from room temperature to 400°C, driving off the adsorbed water (15). Introduction of moist air then produced an immediate reduction of μ. Adsorbed organic substances also tend to lubricate and soften the surface of ceramics. Myristic acid, for instance, enhances surface plasticity and suppresses cracking during sliding of steel on lithium fluoride (7). Chemisorbed oxygen appears to reduce the friction coefficient of titanium carbide by one-half (16).

Particularly pertinent to the present program is a 1977 study reported by Shimura and Tsuya (17), who investigated atmospheric and temperature effects on the friction and wear of some ceramics (tungsten carbide, titanium carbide, chromium carbide, aluminum oxide) and their cermets. It was found that wear rates and coefficients of friction are higher in vacuum than in air. Based on characterization of the wear surfaces, the results were explained in terms of a postulated thin, soft lubricating surface layer which is formed by interaction of the ceramic/cermet with adsorbed moisture.

D. Potential Seal Materials

Although there is little experimental data on friction and wear of ceramics under conditions that would be experienced by the sliding piston seal in an advanced diesel engine (aside from the preceding work by Shimura and Tsuya (17)), the information that is available is fairly consistent in that the carbides are identified as outstanding sliding seal materials. Finkin, Calabrese, and Peterson (18) performed oscillatory pin-on-plate sliding experiments with various ceramic/cermet couples in air at 316-982°C. A Ni-Mo bonded titanium carbide cermet, sliding on dense magnesia-stabilized zirconia was identified as the most promising material couple. A poor second was the Ni-Mo bonded TiC sliding on itself. Zirconia sliding on itself suffered catastrophic wear.

Another study (19) used pad-on-disc sliding experiments at 30-60 m/s, 5-79 psi, and temperatures up to 982°C, in an oxidizing combustion product atmosphere. Thermal shock was a major mechanism of wear. Promising materials were Cr-Mo bonded alumina, silicon carbide, and Ni-Mo bonded titanium carbide.

A recent research program sponsored by the U.S. Department of Energy has been testing ceramic materials for sliding seals in large diesel engines used in stationary applications (20). The goal of the program is to

identify coatings or monolithic ceramics which could resist corrosion and abrasion in engines using substandard fuel and which could permit operation at higher mean effective pressure. This study used pin-on-disc experiments at temperatures up to 427°C in air to assess the wear resistance of various ceramics. In these screening tests the pin and disc were of the same material. For unlubricated service, the best material was aluminum oxide (UHA-99/NTK and A473/Kyocera); SiC, TiC, and B_4C were also judged to be outstanding. By far the lowest coefficient of dry sliding friction was 0.25, for hot-pressed TiC and also for hot-pressed NbC-TaC. A blue oxide which formed on both hot-pressed TiC and a TiC cermet was felt to have a beneficial lubricating effect.

E. Electrical Effects on Hardness and Wear of Carbides

Applied electrical potentials cause significant (up to 60%) changes in the hardness of semiconductors. Particular materials in which these effects have been demonstrated include Si, Ge, InSb, CdS, PbS, InAs, and SiC (21). Usually the phenomenon manifests itself as a decrease of hardness under applied electric fields. It has been ascribed to the influence of the applied field on adsorption of environmental substances on the semiconductor surface (21-23). Since softened surface layers due to adsorption reportedly effect as much as a hundred-fold improvement in wear rates of tungsten, titanium, and chromium carbides (24), there seems to be real potential for a new method of wear control involving electrical effects.

A somewhat different electrical effect on carbide wear rates manifests itself during metal cutting with carbide tools. In this case, current flowing across the tool/workpiece interface causes an increase in tool wear. Thermal emf's due to the high local temperatures generated in metal cutting provide the driving forces for this damaging current flow. In some cases (depending upon the character of the emf's and resistances of the various current pathways in the workpiece/machine tool system), electrical insulation of the cutting tool can improve tool life by 160% (25). Because of the complexity of the problem, the microscopic mechanism by which these thermoelectric currents increase wear rates is not certain. However, there is evidence that adsorption phenomena are also involved in this wear phenomenon, and Postnikov has argued that the electrical effect on wear is due to disruption of (lubricating) adsorbed films by electrical discharges between sliding asperities (26).

II. EXPERIMENTAL APPROACH

A. Background

The research program outlined here is designed to refine the information base regarding carbide seal ring/ceramic cylinder liner combinations for use in the high-performance, near-adiabatic diesel engine. The emphasis is focussed on obtaining quantitative and qualitative information about the wear behavior of candidate carbides run against potential cylinder liner materials (silicon nitride and partially-stabilized zirconia), under conditions representative of the service environment of seal rings in the adiabatic diesel. These conditions include temperatures of 23°C to 800°C, in order to evaluate the severity of wear during and following the startup period. Sliding velocities of up to 10 m/s are pertinent to published concept studies of a lightweight diesel engine for aircraft (3) and for heavy-duty trucks (2); the information now available from work related to large stationary diesels is from tests at 0.3 m/s (20). The wear experiments described here subject the sliding materials to atmospheres that resemble the combustion atmosphere in a diesel cylinder.

In addition to measuring the performance of the best candidate materials under realistic conditions, these experiments also explore the potential benefits of a novel approach to seal wear control. This concept is based on the control of electrical processes in the wear mechanism(s). It has been demonstrated that electrical phenomena can be important in the wear of carbide metal-cutting tools (25), and that imposed electric fields produce significant changes (up to 60%) in the hardness of semiconducting materials such as transition metal carbides. This investigation considers the effect of applied potential fields on the wear behavior, hardness, and fracture toughness of ceramics which might be used for sliding piston seals and cylinder liners.

Hot hardness tests under relevant atmospheric conditions have been carried out as a means to aid in intepreting the wear test results. As noted previously, $H(T)$ and $K_c(T)$ (T = temperature) obtained for a realistic service environment should be key parameters in controlling friction and wear under equivalent conditions.

B. Materials

Candidate cylinder liner materials for the adiabatic diesel are silicon nitride, silicon carbide, and zirconia, with silicon nitride having received most of the emphasis to date. Silicon nitride has good thermal shock resistance, moderate thermal conductivity, reasonably low thermal expansion, and a well-developed technology for production of large parts. However, the strength of the material declines at high temperatures, so that its use is limited to no more than 1100°C. Silicon carbide retains its strength to higher temperatures, but it has a thermal conductivity two to four times higher than silicon nitride which reduces its attractiveness as an insulating cylinder liner. Zirconia, with a thermal conductivity of only 1.9 W/m·K in contrast to silicon nitride at 29.7 W/m·K, is a prime

candidate for cylinder liners. It also retains its strength to much higher temperatures (>1500°C) than silicon nitride, and partially-stabilized grades can be heat treated for transformation toughening. Zirconia has a high coefficient of friction (0.7) in sliding against itself, but the wear rate can be quite low (27). Based on these considerations, the liner materials used for discs in the pin-on-disc experiments performed in the present study were silicon nitride and partially-stabilized zirconia (PSZ).

The pin candidate ring materials used were composed of SiC (discussed above), hot-pressed titanium carbide (TiC), and nickel-molybdenum bonded TiC cermets. Rationales for the TiC systems were based on the limited friction and wear work (18-20) discussed earlier.

Properties of the materials selected are given in Table I.

C. Wear Testing

A special wear testing machine was constructed to permit testing under conditions that are pertinent to the service environment of sliding seal materials in the adiabatic diesel engine. As sketched in Figure 3, the basic configuration of the machine was that of a rotating disc against which three flat-ended pins of identical material slide under controlled normal force. The pin and disc assembly were housed within a heated environmental chamber. Since the pins suffered continuous sliding, while any point on the disc surface experienced only periodic passage of a pin, the pin materials operated under conditions similar to those imposed on a sliding seal ring, and the disc material experienced conditions analogous to those of cylinder liner materials. The wear machine was designed so that the pins and disk were electrically isolated.

Conditions under which the wear tests were run were chosen to represent the adiabatic engine (Table II). The simulated diesel environment (DE) consisted of 7.8% CO_2, 8.9% O_2, and balance N_2; both DE and Ar environments were maintained at 40 psi pressure. Disks and pins were run-in for five minutes at temperature at the start of each test, following evacuation and purging of the system with either DE or Ar and a minimum 20 minute pre-test soak at test temperature. After the initial run-in, the test continued with voltage being varied between -6V and +6V in one volt increments spaced one to two minutes apart.

During the test, the normal load is controlled at 5 pounds, with the disk rotational speed at the point of pin/disk contact being 1 m/sec. Tests were conducted at 23°C, 400°C, and 800°C, for the wear couples shown in Table II.

D. Microhardness Tests

Microhardness tests were performed using a standard Tukon tester totally enclosed in a special environmental chamber. A test load of 800 gm was applied to a high temperature diamond indenter. A heating unit was used

TABLE I

MATERIAL PROPERTIES

Material	E (GPa)	H (GPa)	K_{IC} ($MNm^{-3/2}$)	Grain Size (μm)	Tensile Strength (MPa)
SiC[1]	380	32	4.4	3-5	345
HP TiC[2]	450	32	5.0	30	∿260
Ni-Mo-TiC (K162B)[3]	407	12	∿15	3	1587
Si_3N_4 (NC 132)[4]	310	19	4.8	0.5-3	810
PSZ[5]	210	10	8-15	60	600

[1]Carborundum sintered alpha SiC.

[2]Ceradyne, Inc.

[3]Kennametal Corporation.

[4]Norton Company.

[5]Nilsen (Nilcra) TS grade PSZ.

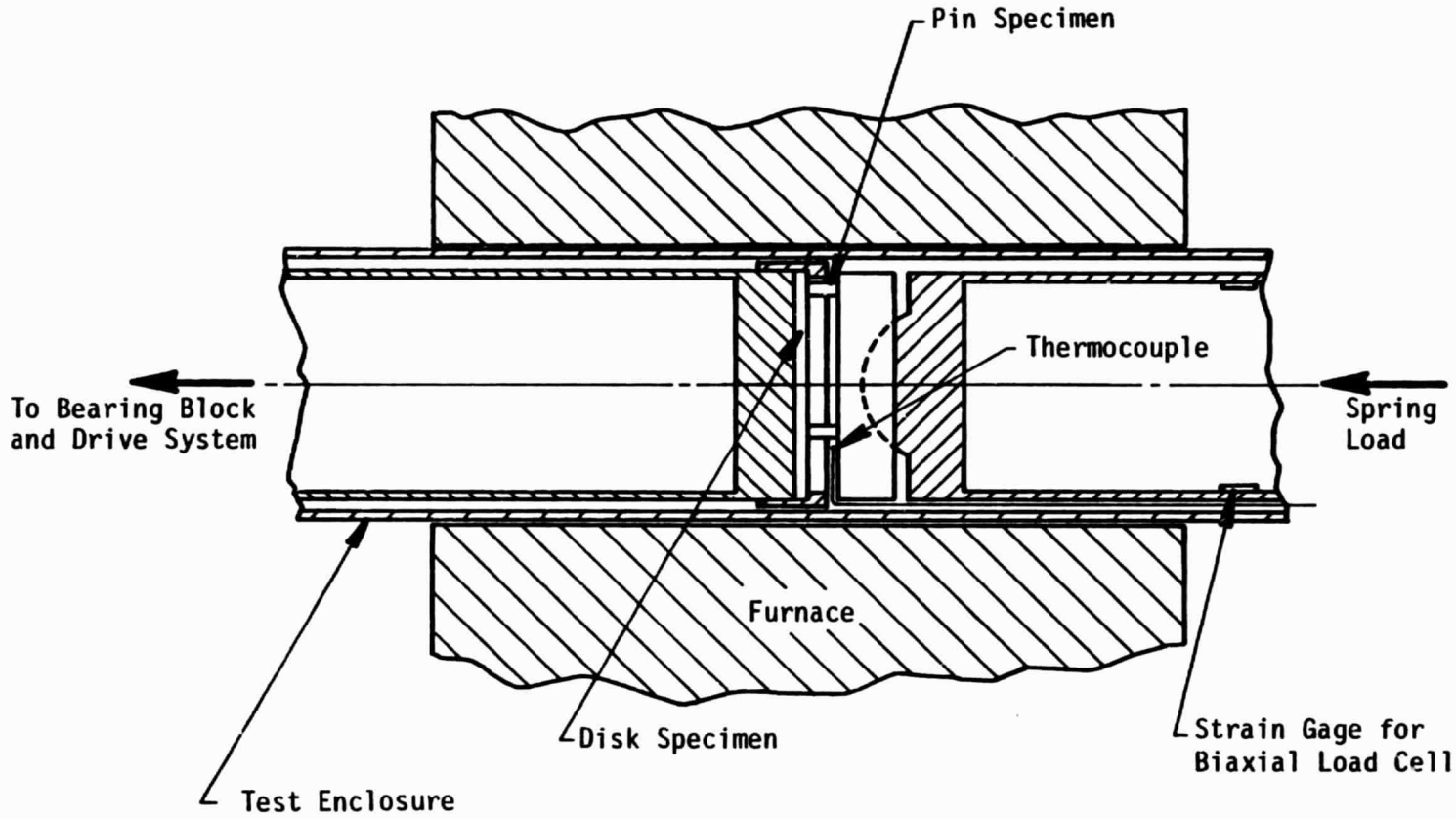

FIGURE 3. Sketch of High-Temperature Friction and Wear Test Apparatus. Disk rotates (drive system not shown) against three stationary pins. Normal load is applied by a loading screw and a low modulus coil spring; strain gages permit measurement of frictional forces.

TABLE II

FRICTION AND WEAR TEST PARAMETERS

Type of Test: Three-Pin on Disk

Load = 5 pounds, Internal pressure = 40 psi

T = 23, 400, 800 (°C)

Environment: Simulated Diesel Exhaust, Dry Argon

Voltage = -6 to +6 (volts)

Material Couples (disk/pin):

PSZ/SiC
PSZ/TiC
PSZ/Ni-Mo-TiC (K 162B)

NC 132/SiC
NC 132/TiC
NC 132/Ni-Mo-TiC (K 162B)

to bring the ceramic specimens to the test temperature, which was ascertained by means of a thermocouple affixed near the indentation site. The indenter was electrically insulated from the test specimen.

Prior to testing, the chamber was purged for several hours with either DE or Ar environments. Indentation tests were performed at 23, 200, 400, 600, and 800°C in each atmosphere; at each temperature, indenter/specimen electric potential was varied between -6V and +6V. Certain electric potential tests were repeated in 100% relative humidity air to try and enhance the effect of potential. Indents and their associated radial corner cracks were used to evaluate hardness and fracture toughness, respectively, the latter according to the analysis of Evans and Charles (28).

E. Wear Characterization

Prior to testing, both pins and disks were carefully polished to a 0.5 μm diamond finish. There always was a slight error in parallelism between pins and disk once a test began, and so on each pin, a small wear flat was produced (tests did not begin until this flat was run-in and basically stable). For subsequent wear characterization, the polished surfaces provided reference "no-damage" regions, while the boundaries of the pin flats constituted regions in which damage development could be observed from its inception to equilibrium wear. Similarly, the width of the annular wear track on each disk slowly expanded with the pin flats, so that again, by tracking across the boundary one passed quickly from no damage through the various stages of damage development leading to equilibrium wear.

Scanning electron microscopy was the principal technique used to characterize wear mechanisms. In some cases, energy dispersive spectroscopy (EDS) was employed to characterize wear particles and transfer layers.

Additionally, wear rates were characterized by weighing pins before and after testing in a precision balance (these tests were frequently compromised by chipping and/or oxidation weight gain). A more reliable measure of weight loss was provided by profiliometry of the disk wear tracks. These latter measurements provided the main body of reliable wear rate data.

III. RESULTS

A. Indentation Tests

1. Hardness

The effect of temperature (T) and environment upon hardness is shown for each individual ceramic in Figures 4-8. In all cases, H decreases with increasing T, and the effect of environment, though evident in particular for TiC (Figure 8), is not great. On the other hand, it is very instructive to compare the H(T) curves on the basis of material, for a given environment, as shown in Figure 9 for DE. From the latter, it is clear that there exist large differences in hardness over the entire temperature range. At 800°C, the SiC and NC 132 disk materials are roughly twice as hard as the three pin materials.

Essentially no effect of electric potential upon hardness was observed. An example is shown in Figure 10 for SiC tested in air at 23°C; the open and closed circles represent two different test series run under identical conditions.

2. Fracture Toughness

As shown in Figures 11-13, environment plays a significant role in the fracture toughness of ceramics; further, the effect is qualitatively different from one ceramic system to another. For NC 132, for example (Figure 11), $K_c(T)$ is higher in Ar than in DE for all T, while showing a maximum at $T \simeq 400°C$ in both environments. In the case of SiC, on the other hand, $K_c(T)$ is lower in Ar than in DE over most of the temperature range of interest, and there is a maximum in both curves at $T \simeq 500°C$.

The case for TiC (Figure 13) appears to be rather more complex. As T increases, K_c in DE rises, while that in Ar falls, the greatest differential occurring at $T \simeq 200°C$. Above this temperature, K_c falls precipitously in DE, while in Ar staying constant at a low level before rising sharply at $T = 500°C$. Data could not be obtained at higher temperatures for the TiC, due to degradation of the surface. In addition, indents in PSZ and NiMo-TiC did not crack at the imposed load of 800 gm, hence K_c could not be measured. Subsequent hardness tests at higher indentation loads will be required for these materials in order to produce microfracture (K_c) data.

The DE $K_c(T)$ results for these three materials, fit to smooth curves, are shown in Figure 14. Wide quantitative and qualitative differences are apparent.

The only instance in which electric potential seemed to alter K_c, SiC tested in humid air at 23°C, is shown in Figure 15. Here, for two separate test series (open and closed circles), K_c apparently experiences an approximate 30% enhancement at a potential of -4.5 to -5 volts. It is

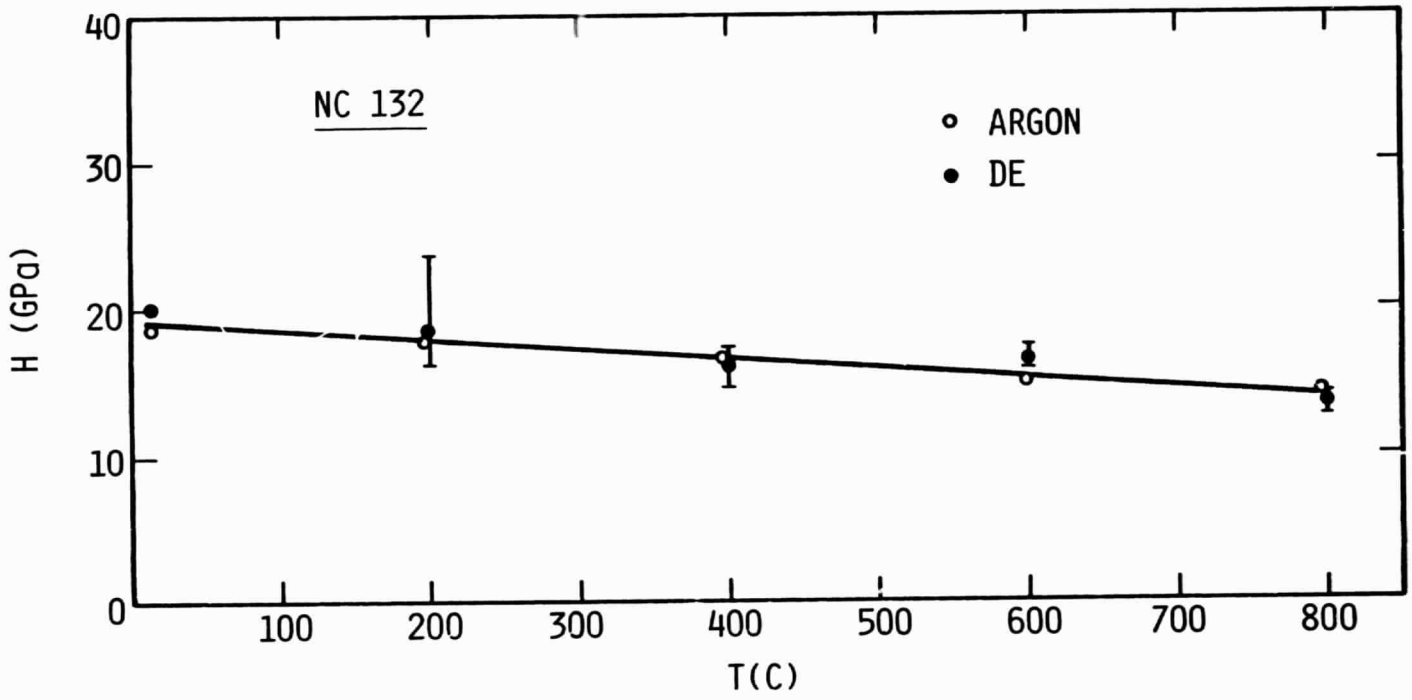

Figure 4. Hardness Versus Temperature for NC 132 in DE and Ar.

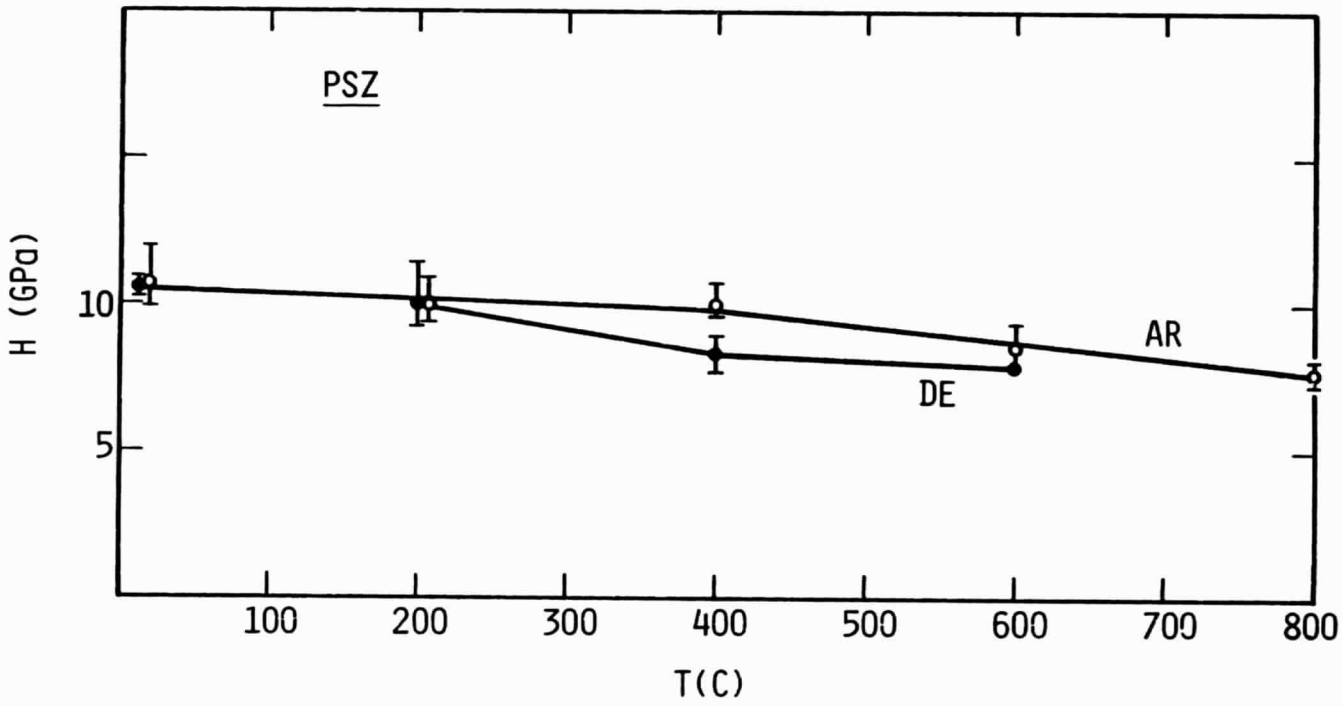

Figure 5. Hardness Versus Temperature for PSZ in DE and Ar.

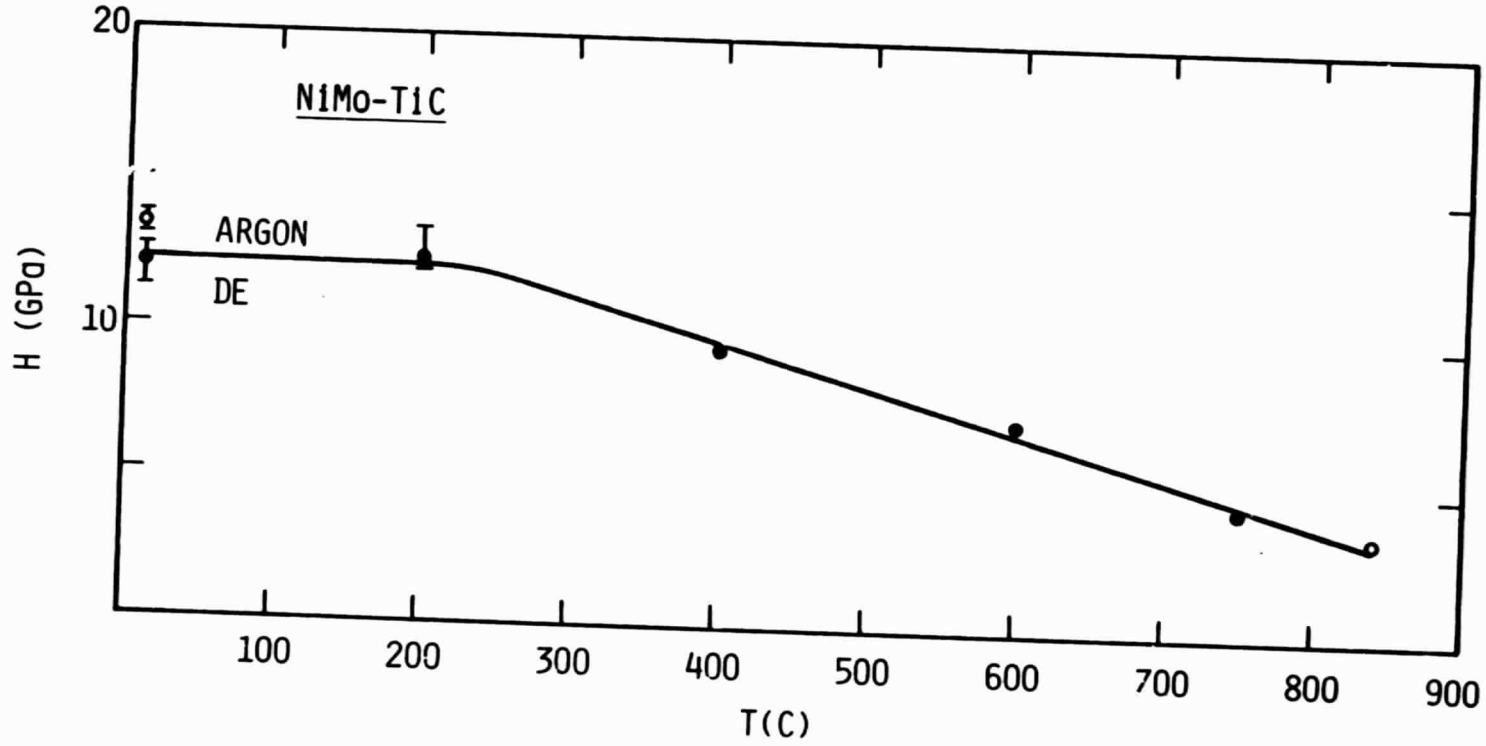

Figure 6. Hardness Versus Temperature for NiMo-TiC in DE and Ar.

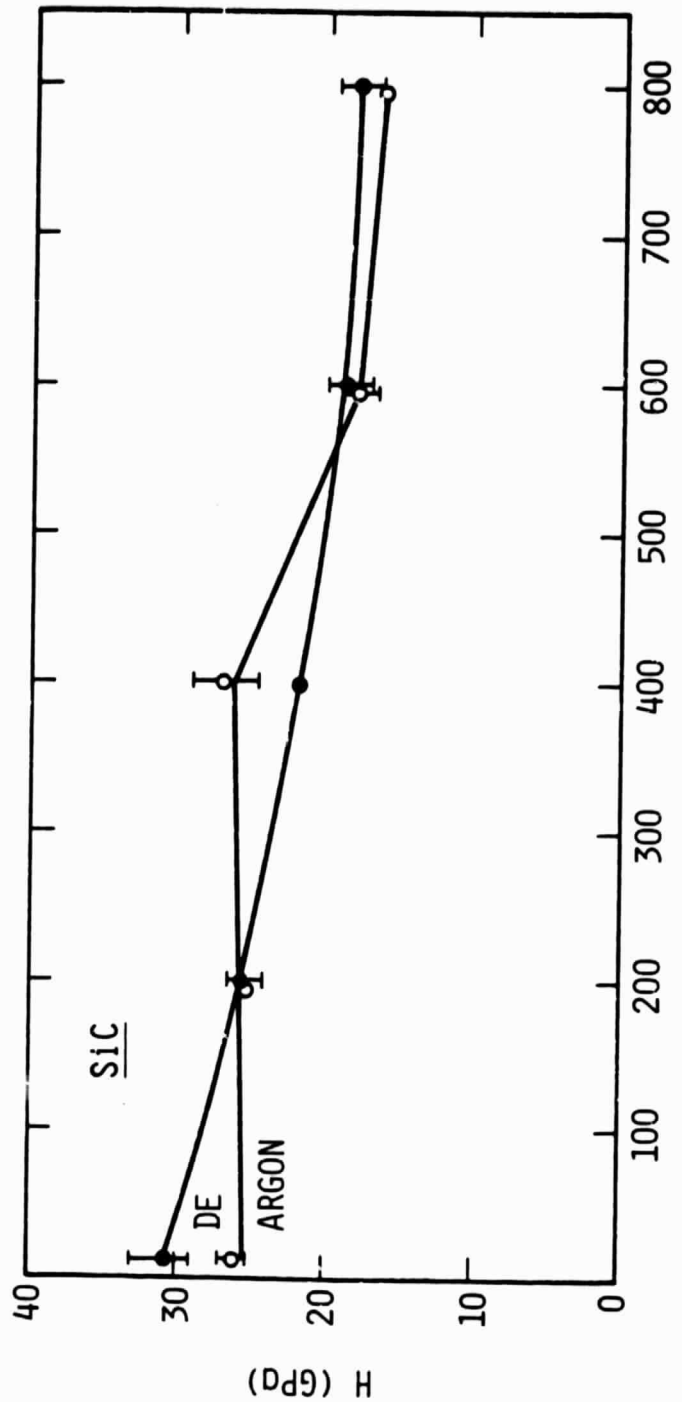

Figure 7. Hardness Versus Temperature for SiC in DE and Ar.

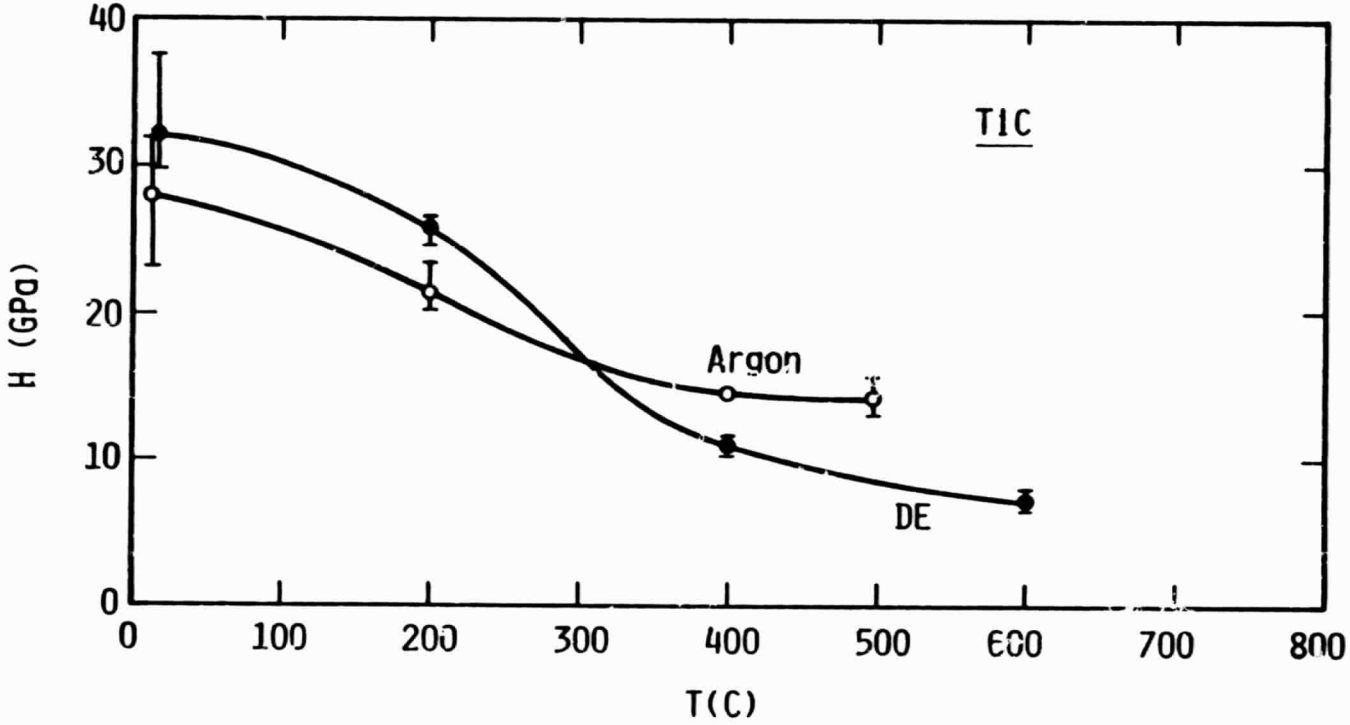

Figure 8. Hardness Versus Temperature for TiC in DE and Ar.

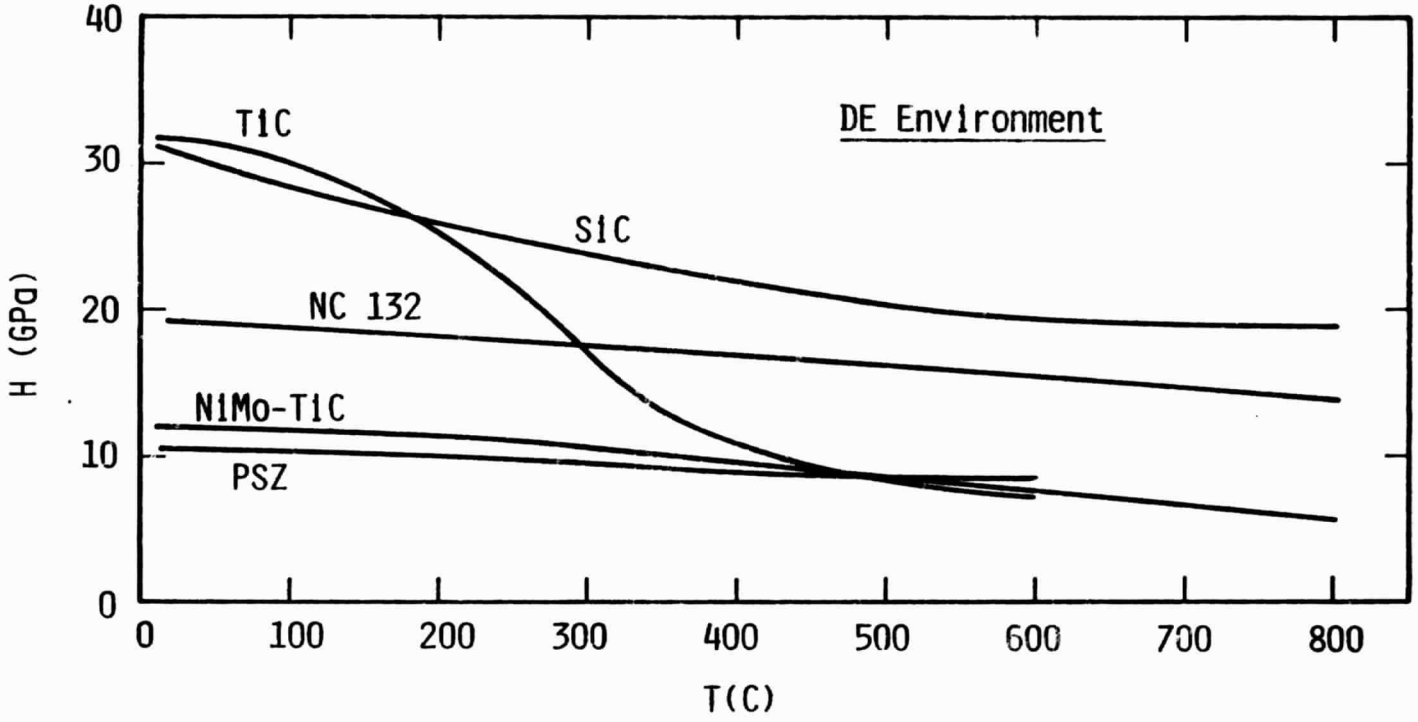

Figure 9. Hardness Versus Temperature for All Materials in DE.

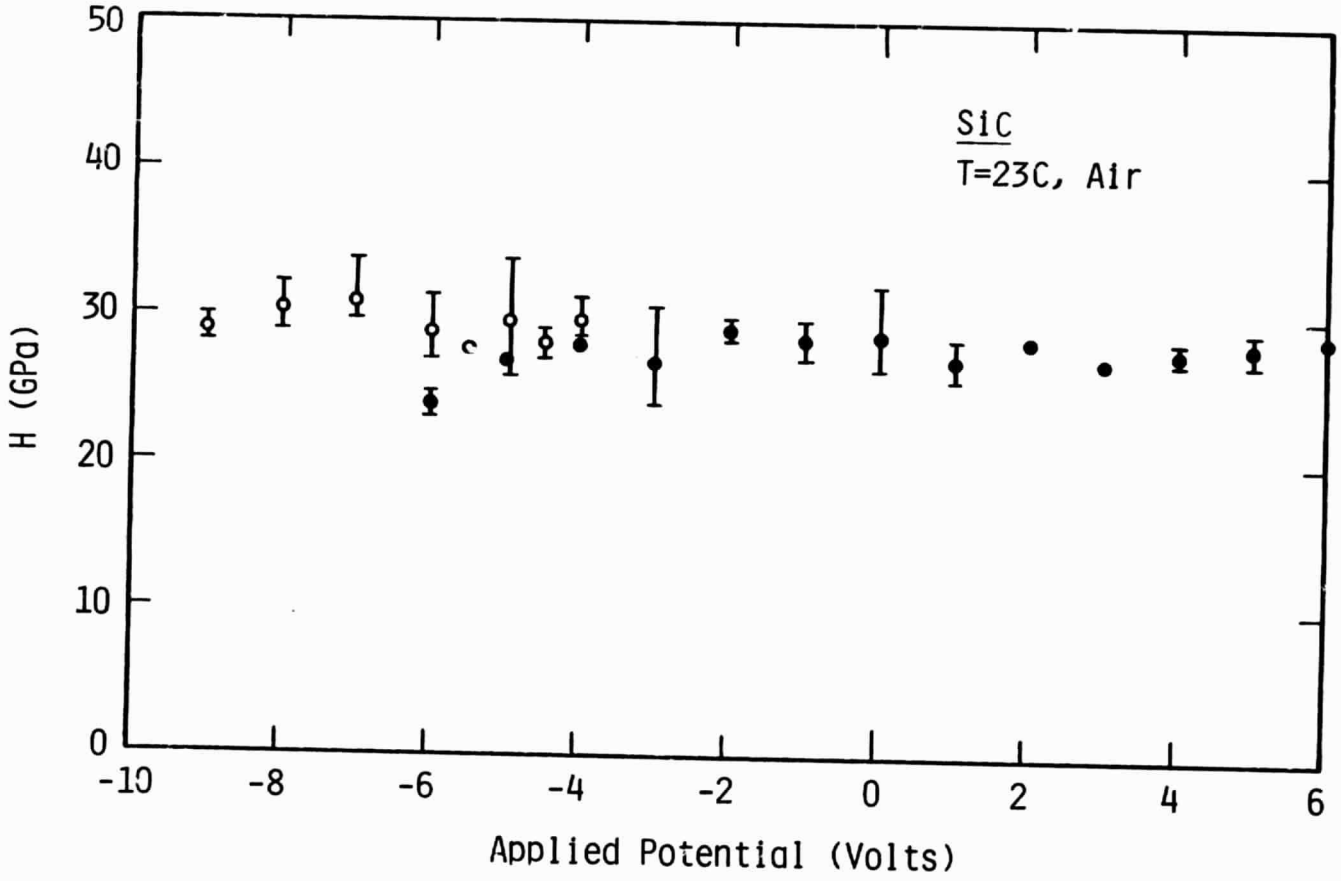

Figure 10. Hardness Versus Applied Electrical Potential for SiC at 23°C in Humid Air.

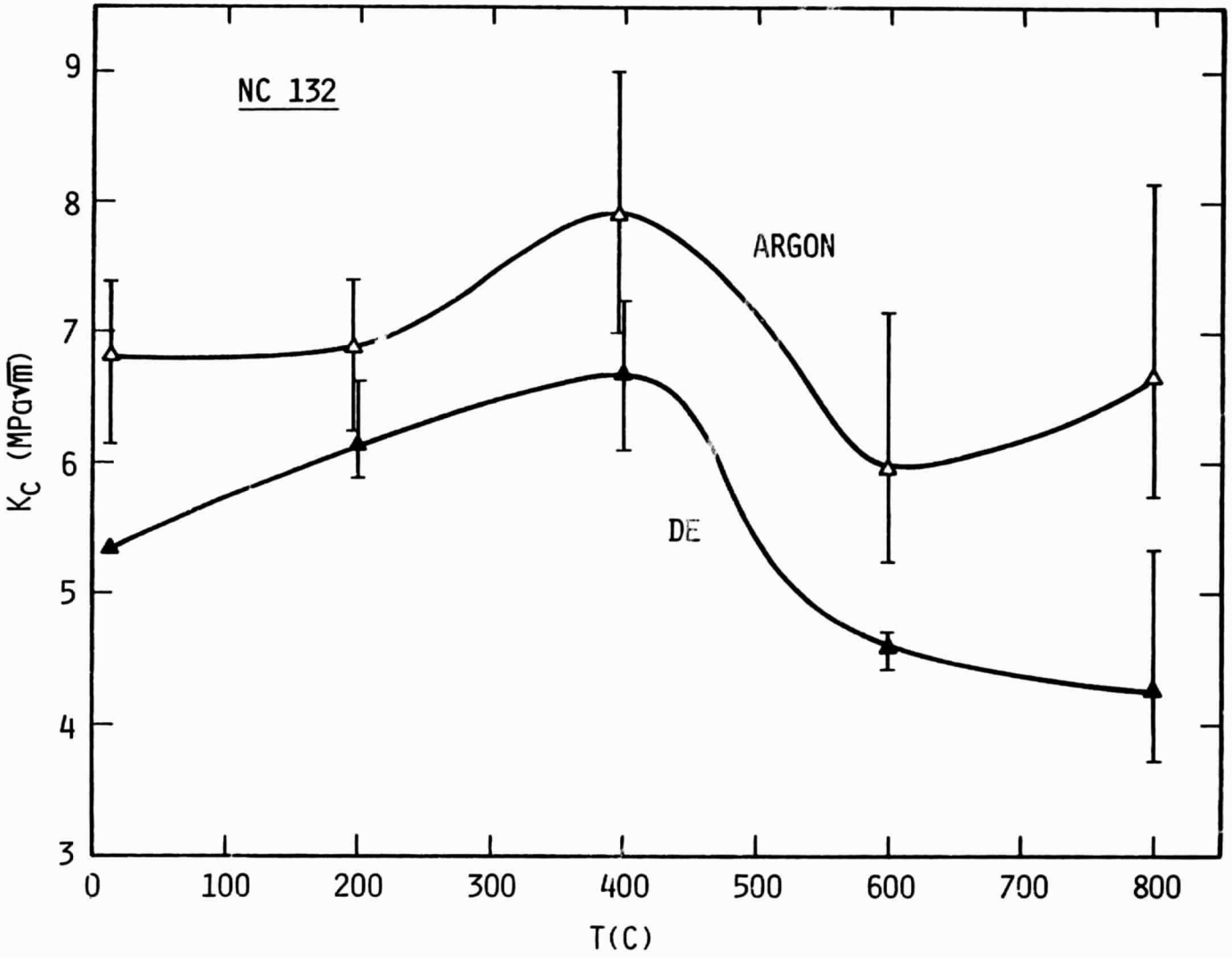

Figure 11. Fracture Toughness Versus Temperature for NC 132 in DE and Ar.

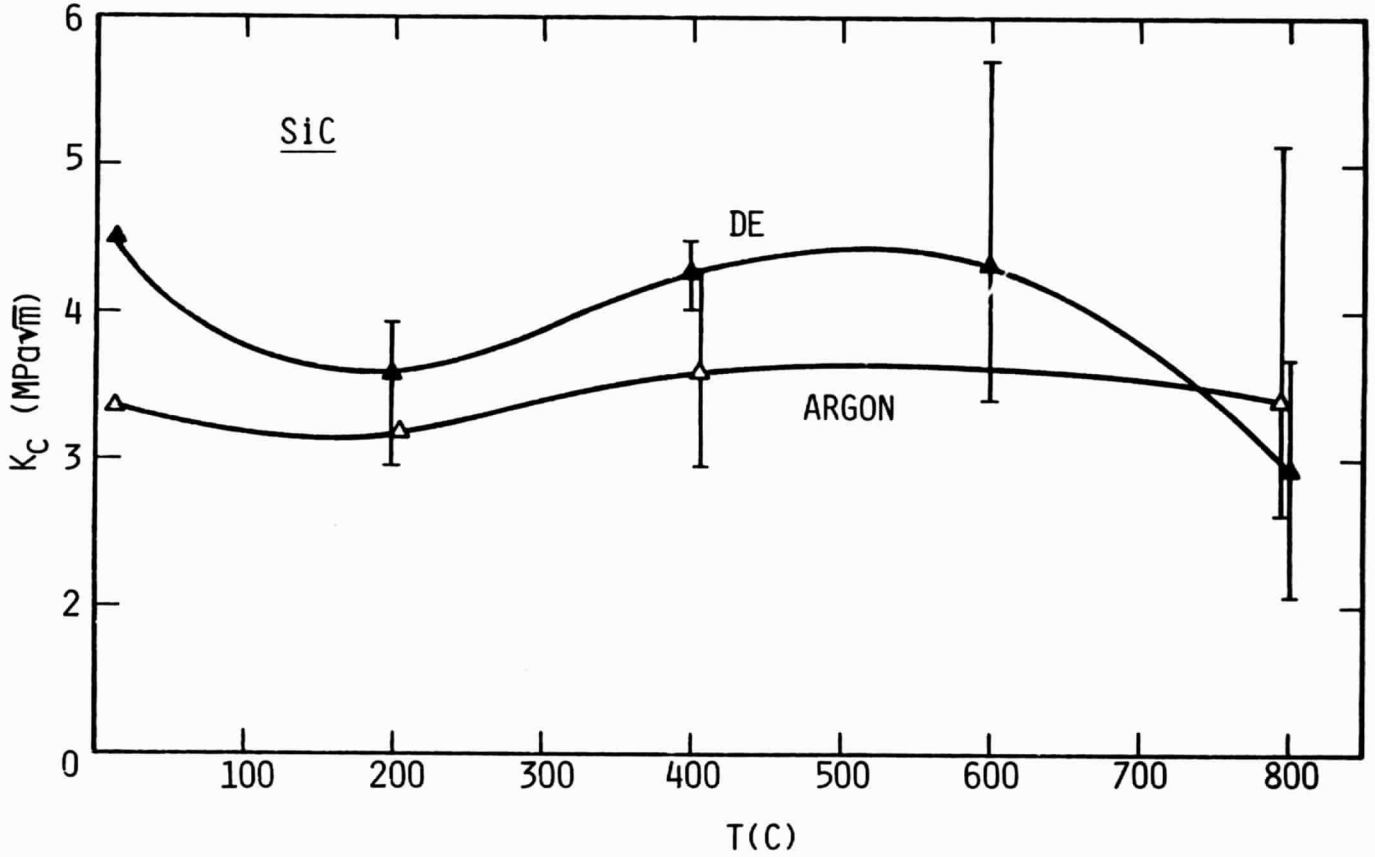

Figure 12. Fracture Toughness Versus Temperature for SiC in DE and Ar.

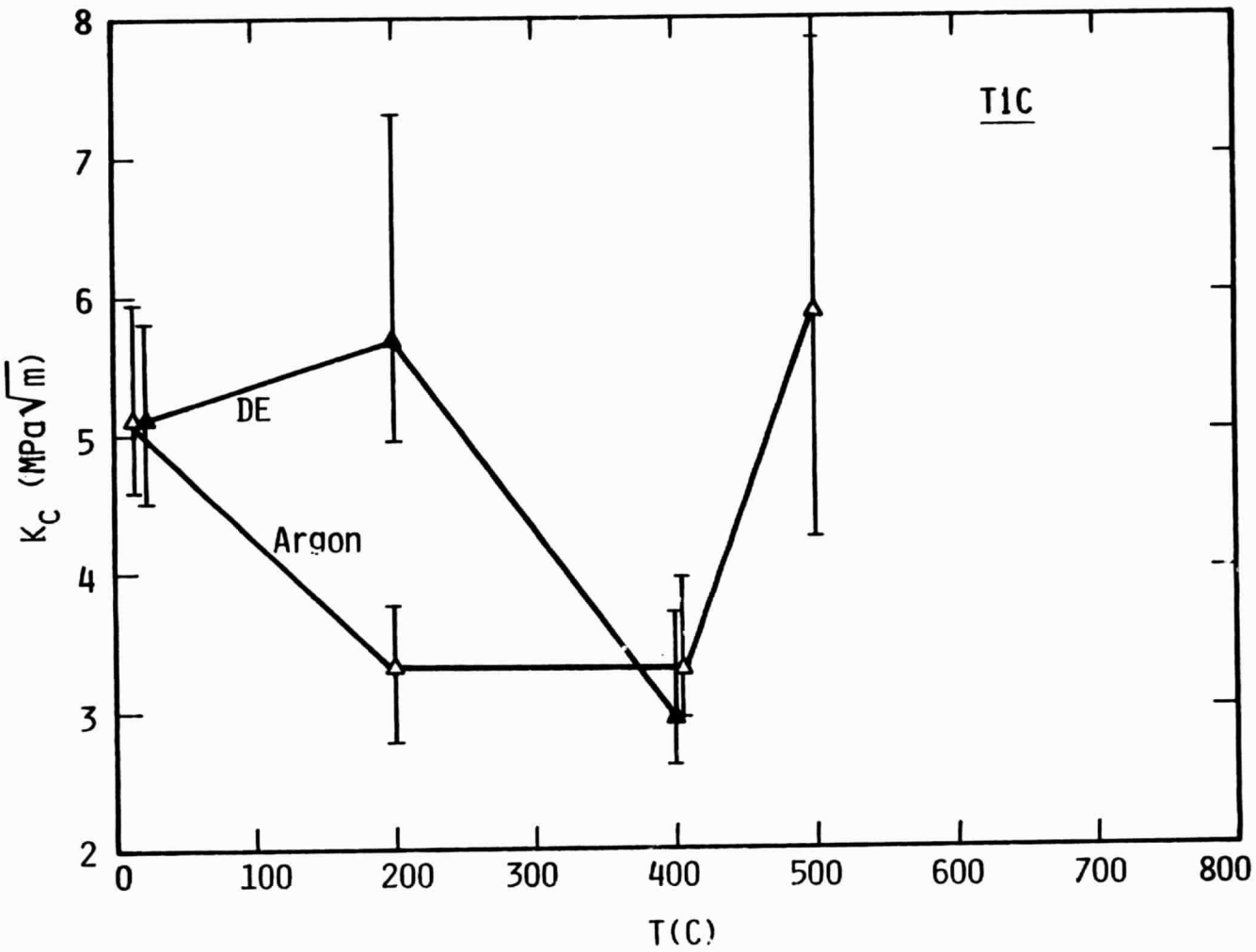

Figure 13. Fracture Toughness Versus Temperature for TiC in DE and Ar.

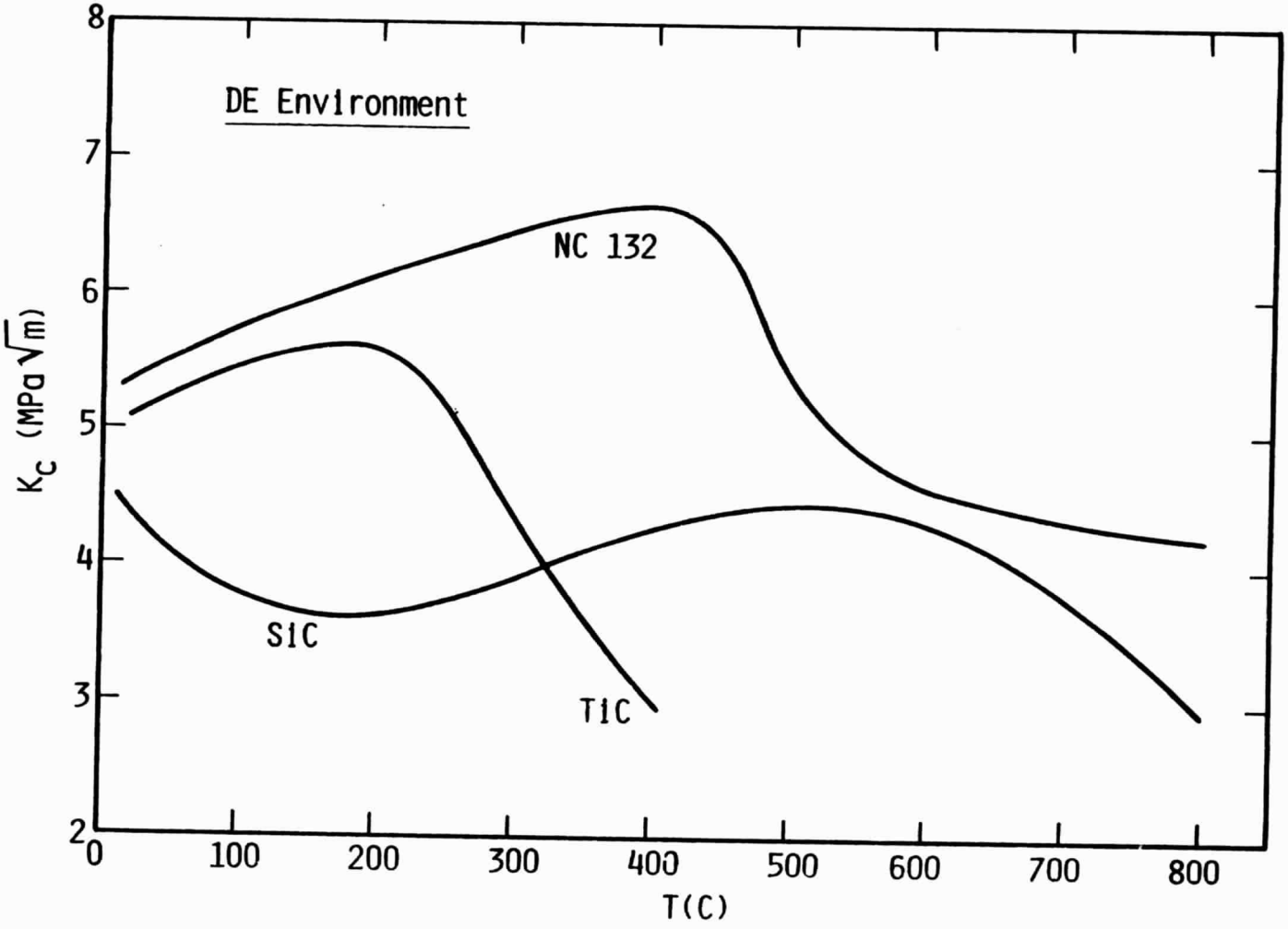

Figure 14. Fracture Toughness Versus Temperature for NC 132, SiC, and TiC in DE.

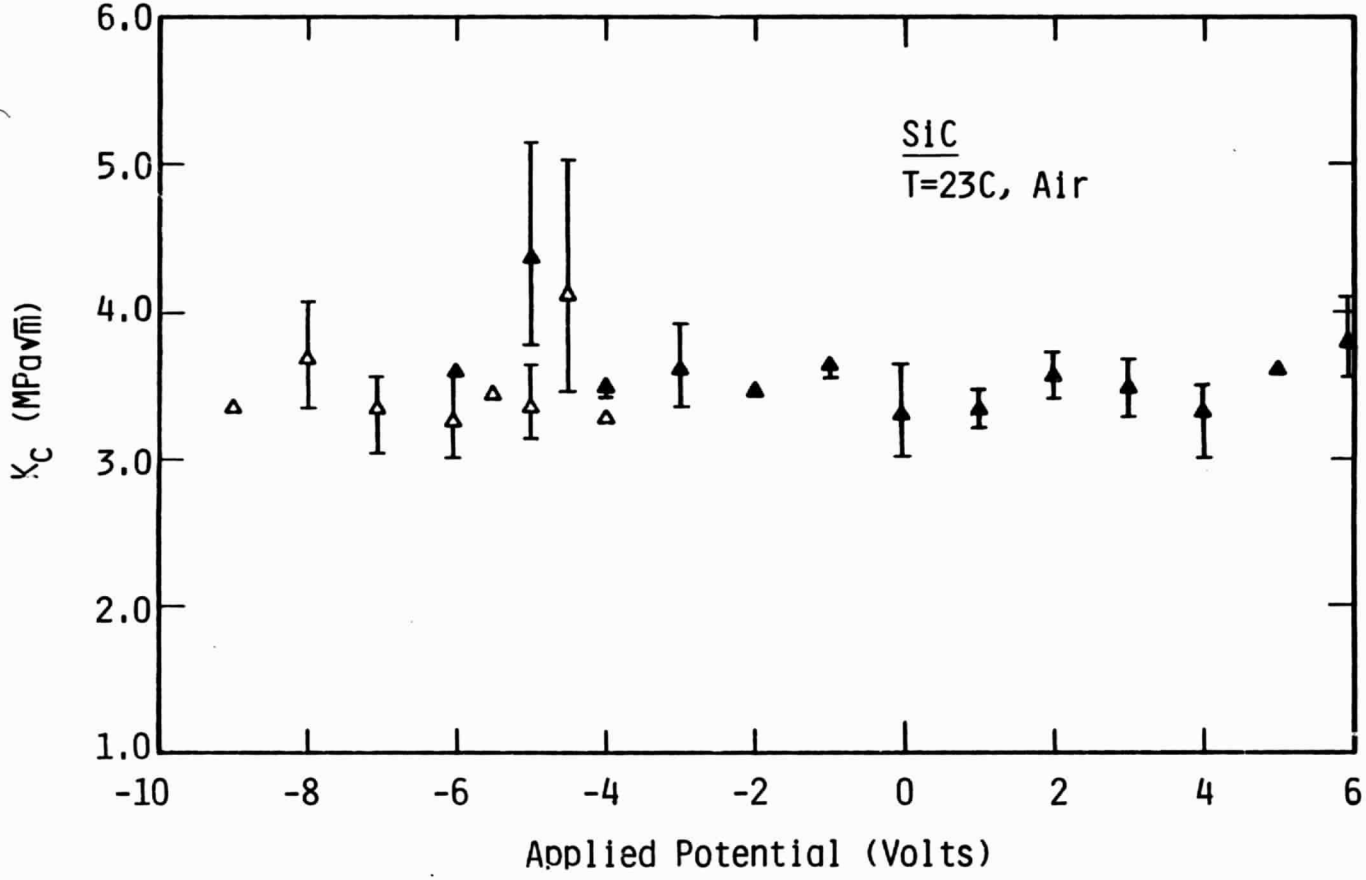

Figure 15. Fracture Toughness Versus Applied Electrical Potential for SiC at 23°C in Humid Air.

interesting to note that within this narrow voltage band, scatter in the measured K_C values is nearly triple that for other potentials.

B. Wear Tests

1. Friction Coefficients

Friction coefficients for the six individual pin/disk couples in DE and Ar are shown as functions of temperature in Figures 16-21. It can be seen that μ ranges from a high value of more than 1.0 (SiC pins/NC 132 disk in DE at 800°C), to a minimum of 0.24 (K162B pins/NC 132 disk, again in DE at 800°C). However, a more effective mode of presentation for subsequent discussion is to combine the curves for all three pin materials sliding on one disk in a given environment as in Figures 22-25.

For example, μ lies between 0.6 and 0.8 for all three pin materials run against PSZ in Ar (Figure 22). For NC 132 disks in the same environment (Figure 23), the situation is only marginally different; as T increases, μ for all pins decreases slightly, from $\sim$0.8 to $\sim$0.6. This simple behavior is altered drastically, however, by running in DE.

As shown in Figure 24, for PSZ disks in DE, μ rises rapidly with T for SiC and TiC, peaks at $\sim$400°C, and then decreases rapidly with further increase in T. For K162B, on the other hand, μ decreases monotonically from its initial room temperature value of $\sim$0.9, to a low of $\sim$0.45 at 800°C. For NC 132 disks in DE (Figure 25), the K162B material behaves much as it does for PSZ disks in the same environment, dropping from $\sim$0.75 at 23°C to 0.24 at 800°C. However, μ(T) for SiC and TiC increase monotonically; there is no mid-temperature peak, and at 800°C, μ is quite high for both.

In none of these tests was there any measurable effect of varying the pin/disk electrical potential.

2. Wear Rates

Because of the oxidation and chipping problems associated with wear measurements on the pins, this section will deal with wear rates ($\dot{W}$) for disks. Pin wear will be characterized qualitatively in the following section.

As shown in Figure 26, $\dot{W}$ for PSZ disks run in Ar increases with T for all three pin materials. It is interesting that at room temperature in Ar, SiC pins produce essentially no disk wear. For the same disk material in DE (Figure 27), wear against SiC pins is again low at 23°C, but is catastrophic at 800°C. On the other hand, K162B and TiC pins produce remarkably low disk wear at 800°C.

For NC 132 disks (Figure 28), wear rate data is less complete, due to disk damage during some of the Ar tests. Nevertheless, some interesting trends emerge. In particular, the DE tests indicate rapid disk wear by SiC pins with increasing temperature, while the disk wear rate is very low against TiC, and essentially unmeasurable against K162B, over the entire temperature range of interest. It should be noted that NC 132 disks run against K162B pins in Ar also exhibit low wear rates at 800°C.

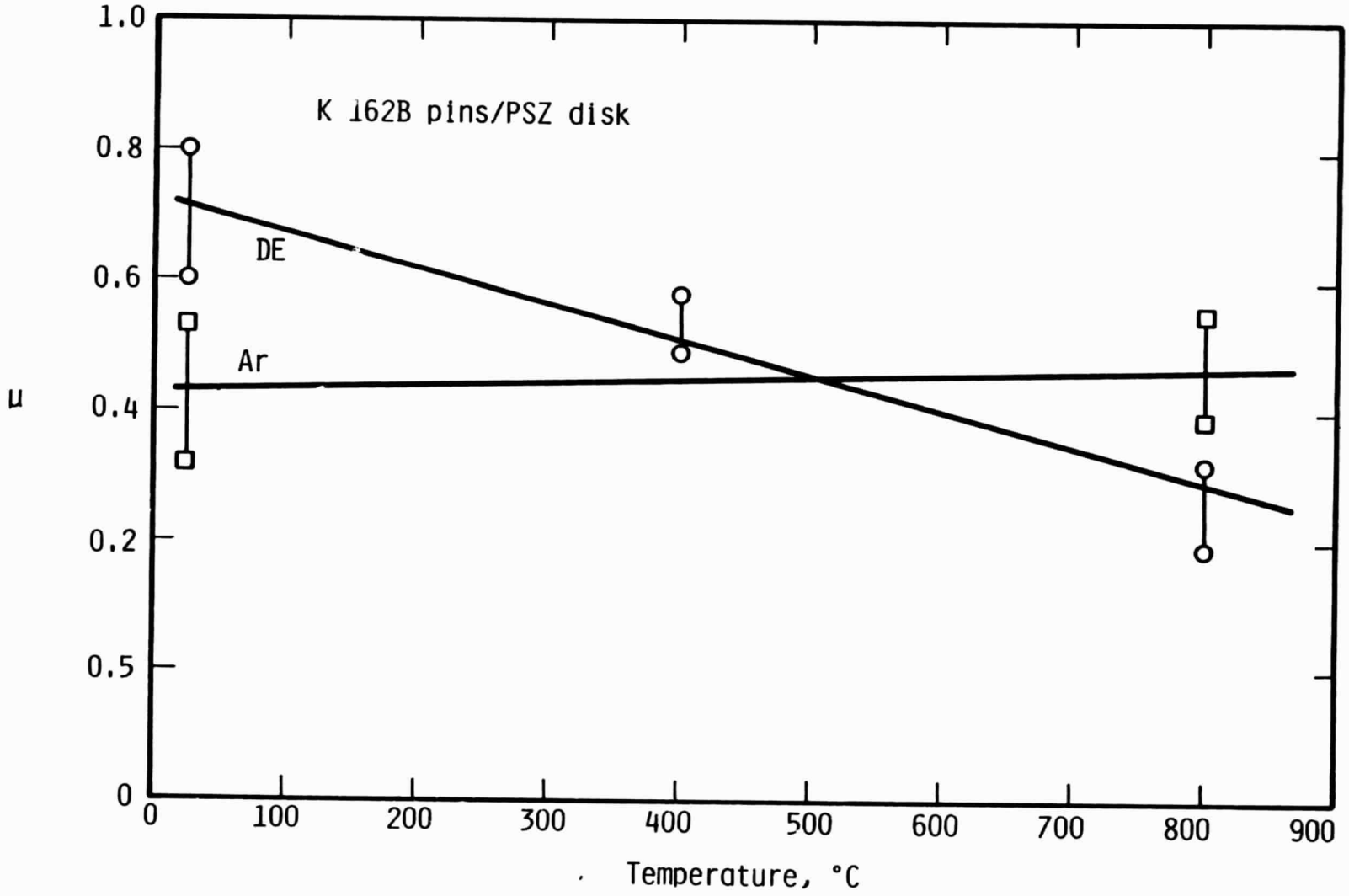

Figure 16. Friction Coefficient Versus Temperature for K162B Pins/PSZ Disk in DE and Ar.

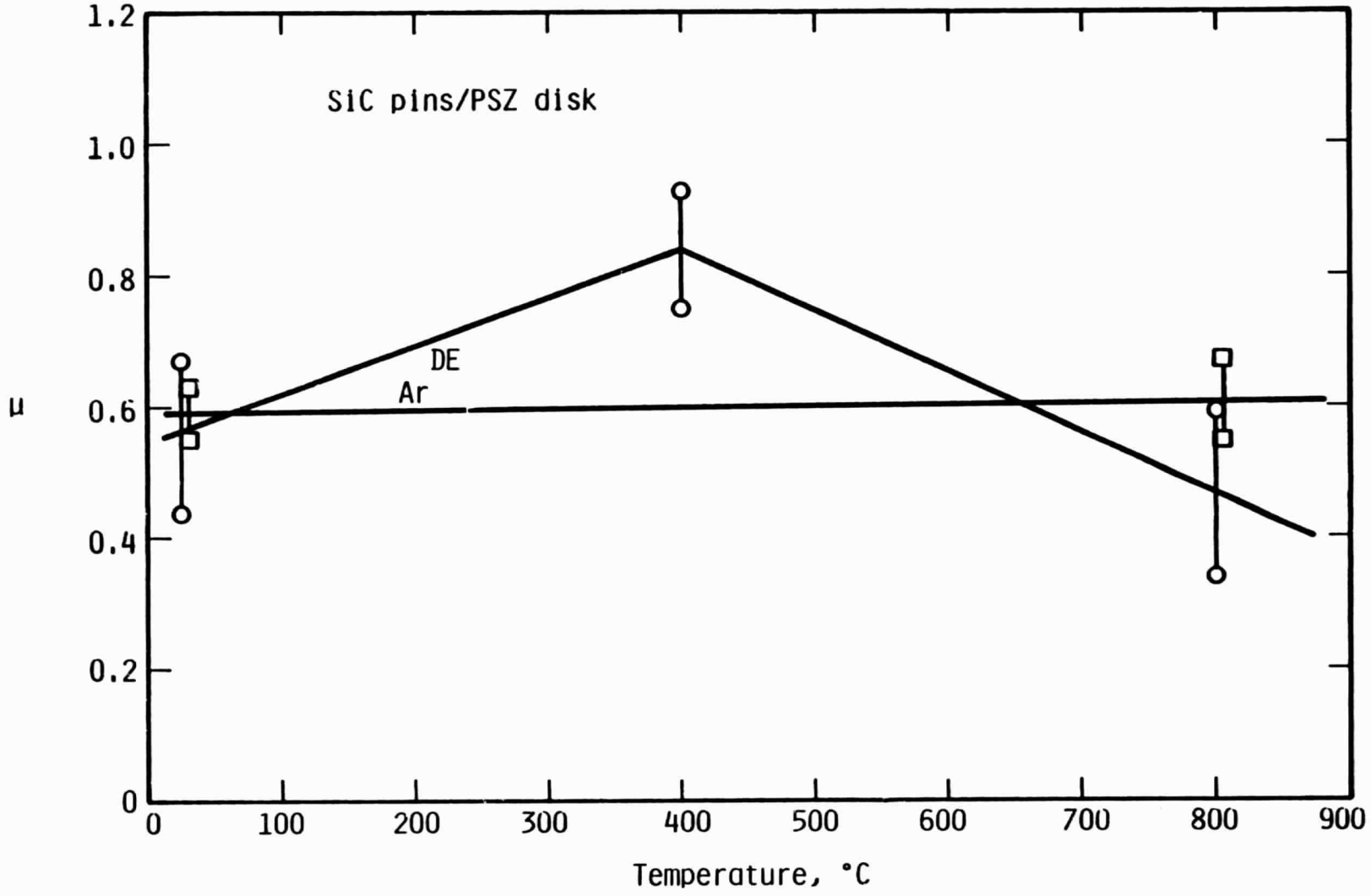

Figure 17. Friction Coefficient Versus Temperature for SiC Pins/PSZ Disk in DE and Ar.

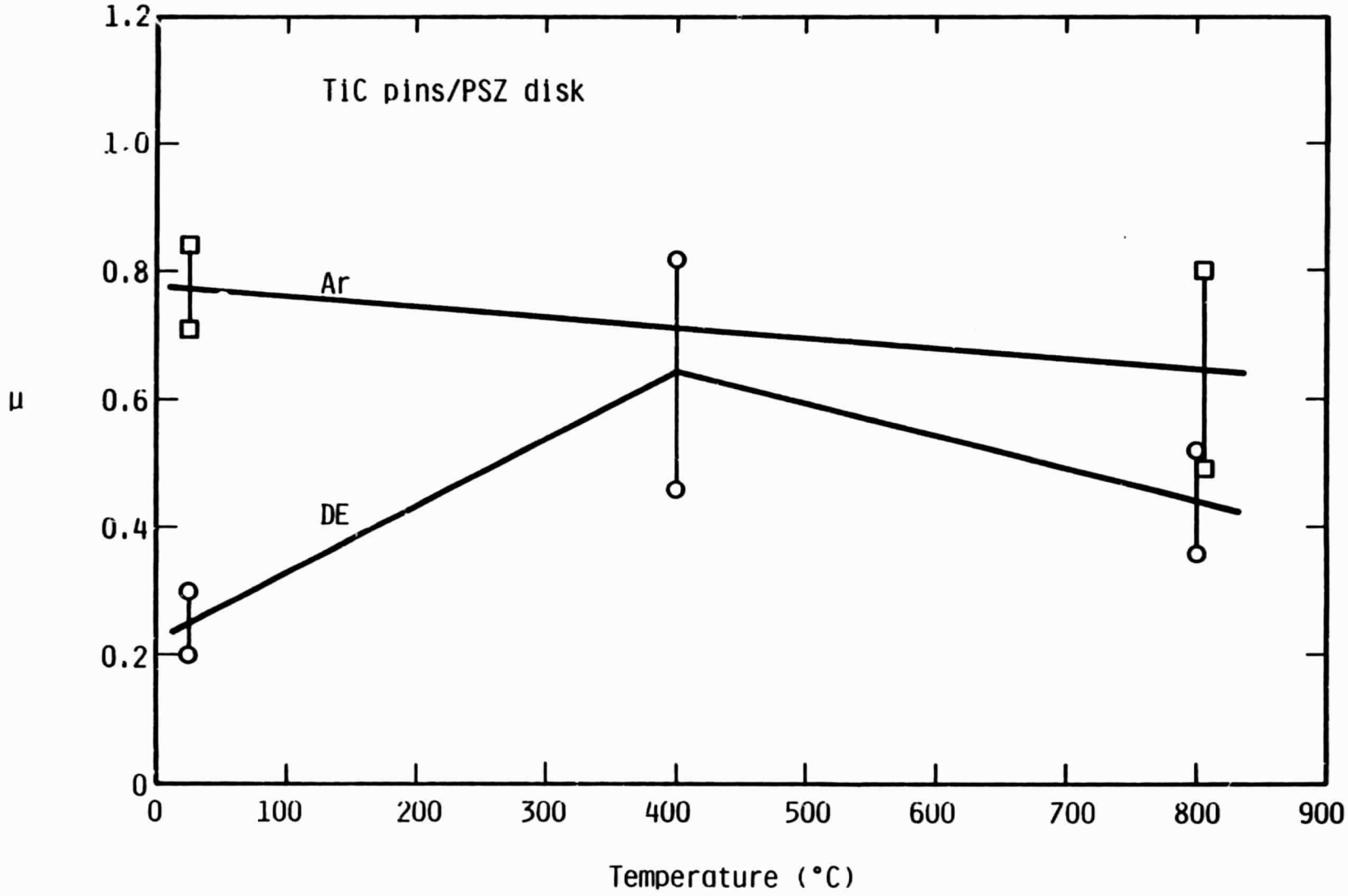

Figure 18. Friction Coefficient Versus Temperature for TiC Pins/PSZ Disk in DE and Ar.

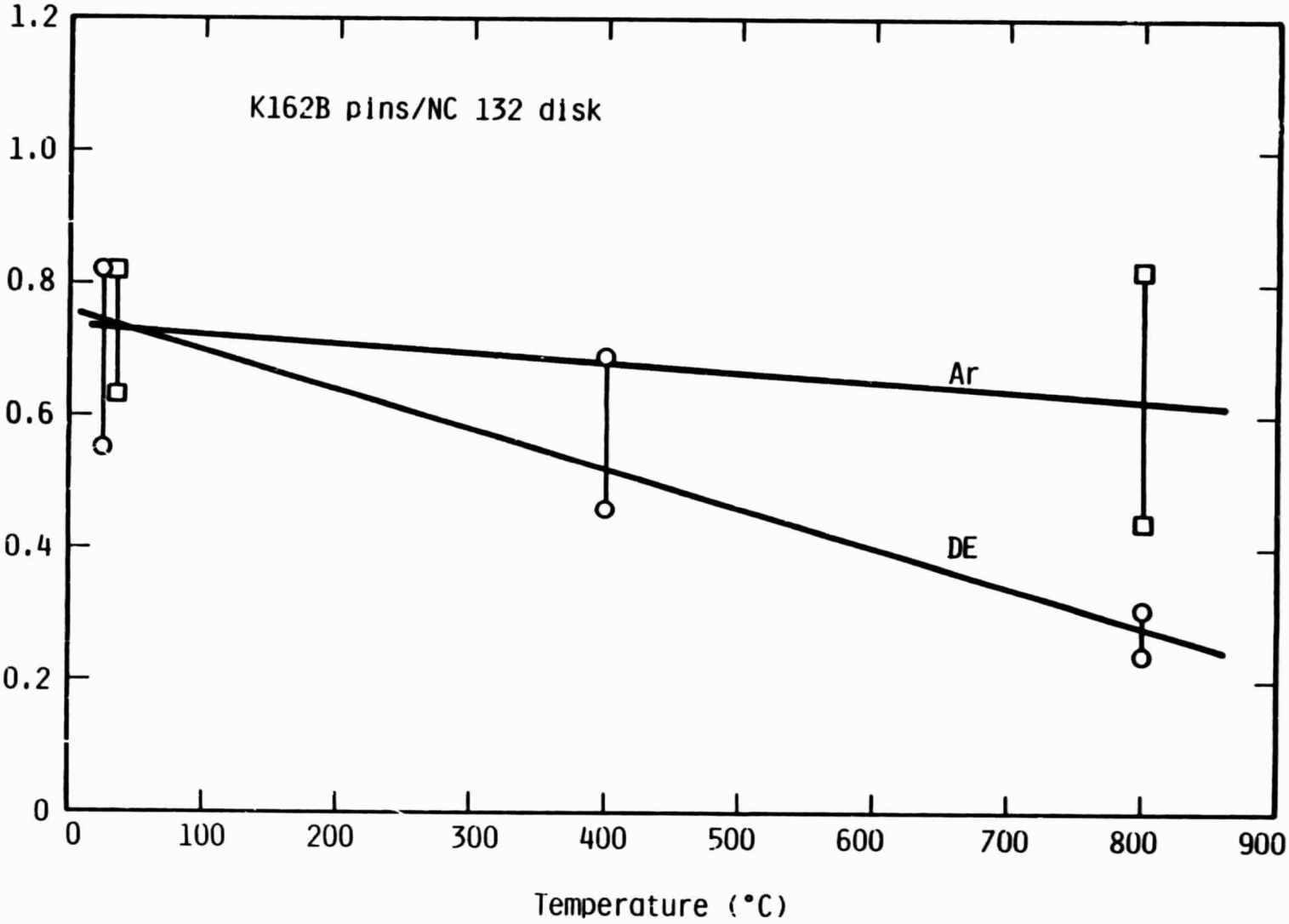

Figure 19. Friction Coefficient Versus Temperature for K162B Pins/NC 132 Disk in DE and Ar.

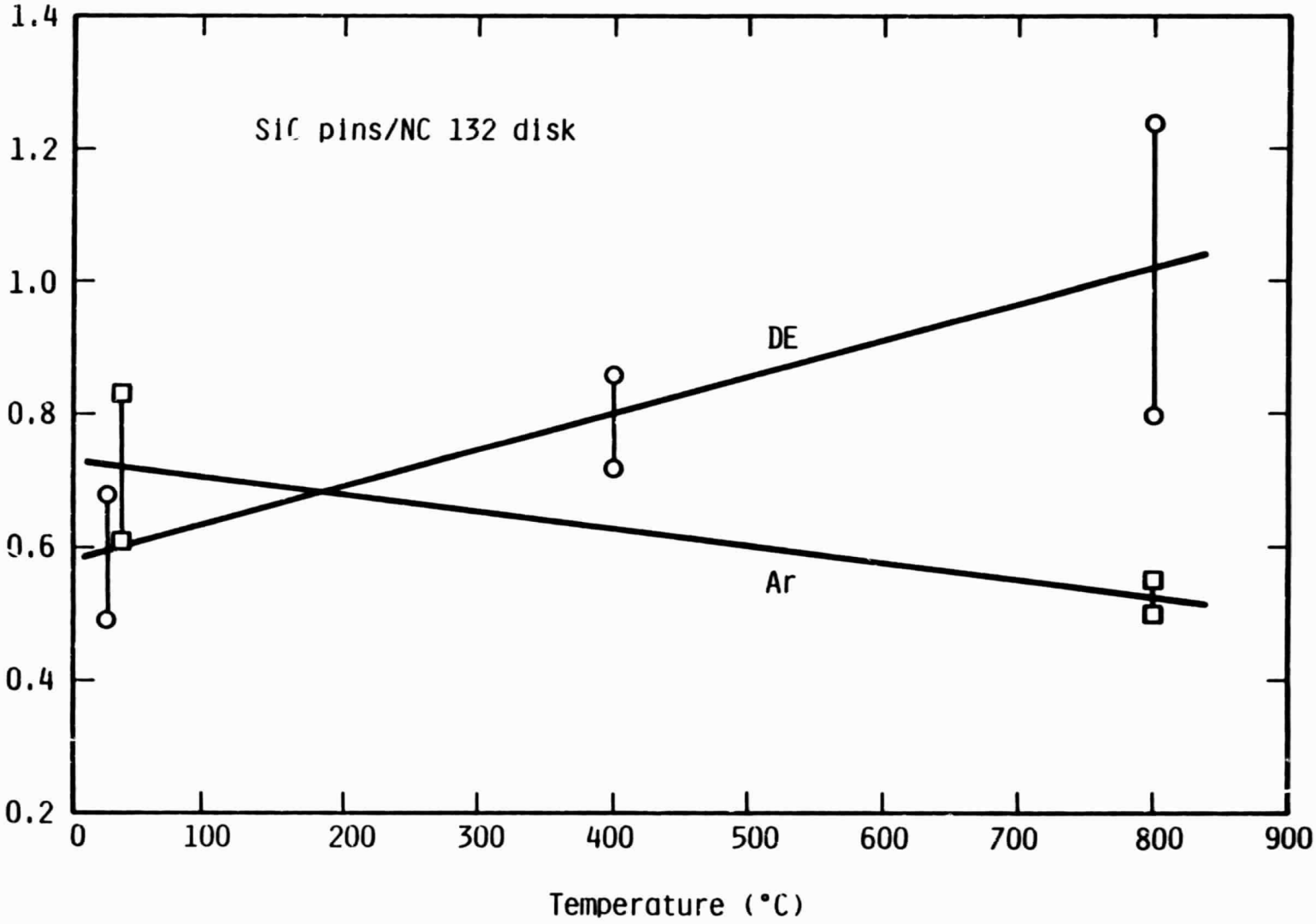

Figure 20. Friction Coefficient Versus Temperature for SiC Pins/NC 132 Disk in DE and Ar.

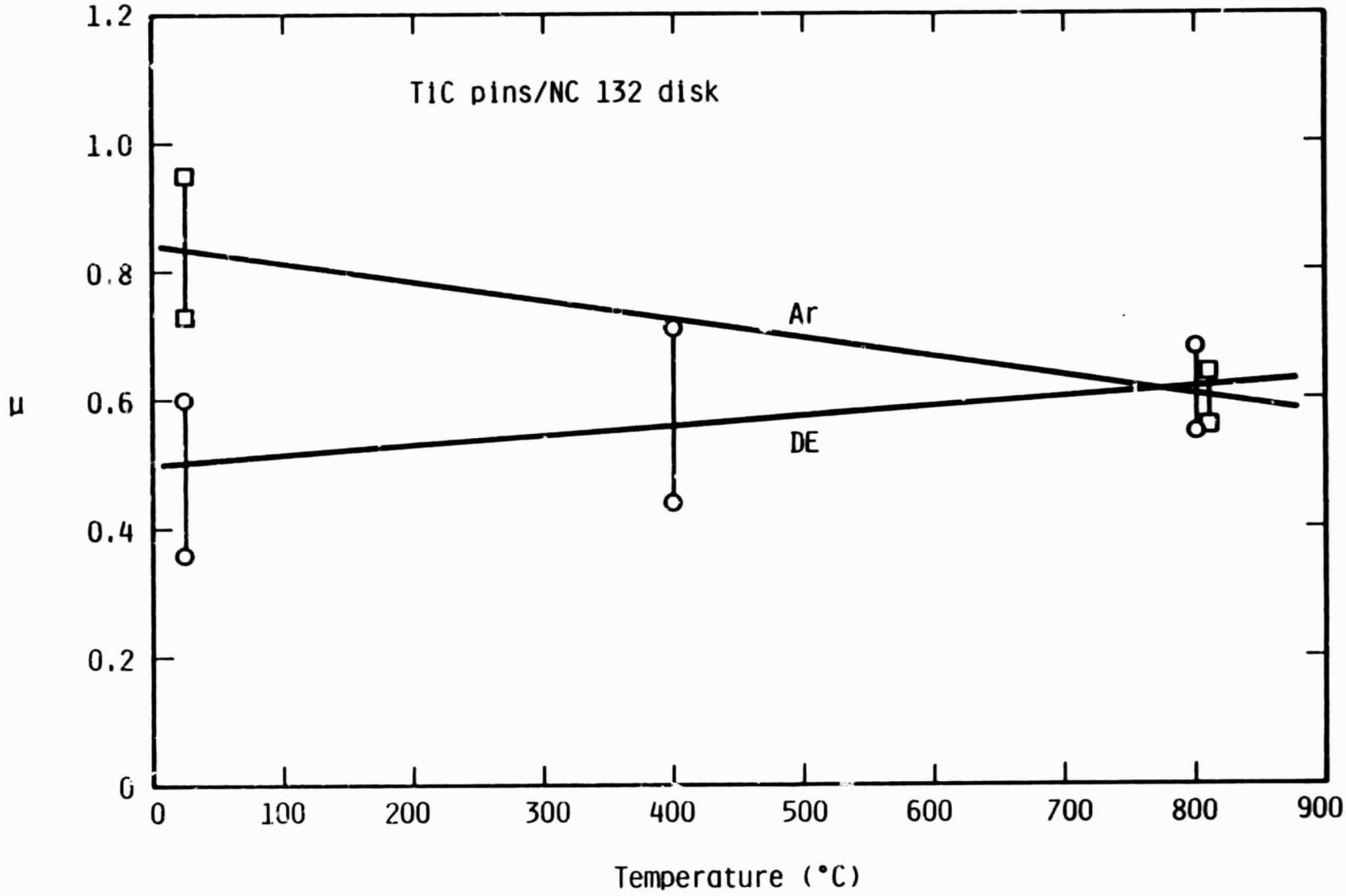

Figure 21. Friction Coefficient Versus Temperature for TiC Pins/NC 132 Disk in DE and Ar.

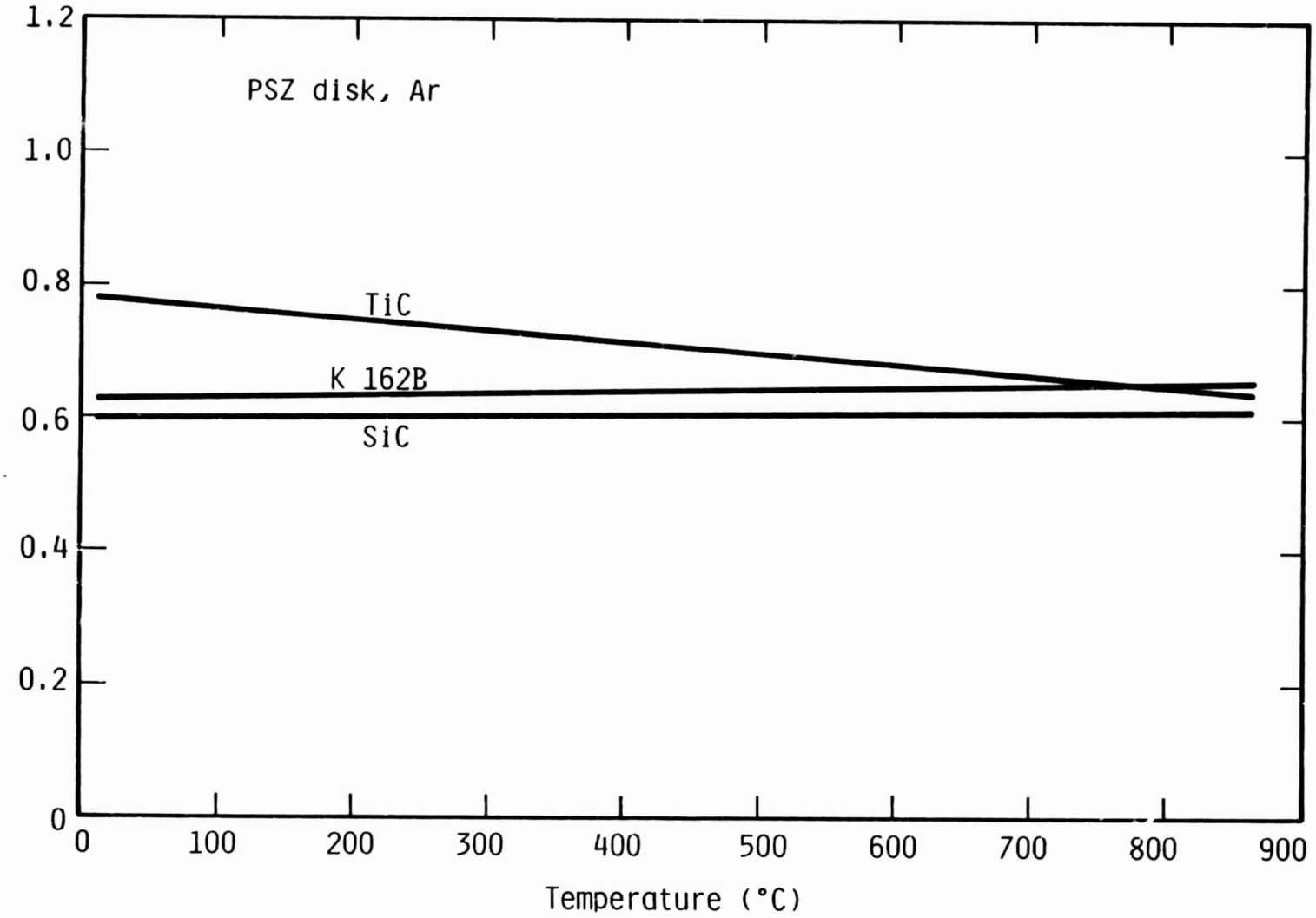

Figure 22. Friction Coefficient Versus Temperature for All Pin Materials on PSZ Disks in Ar.

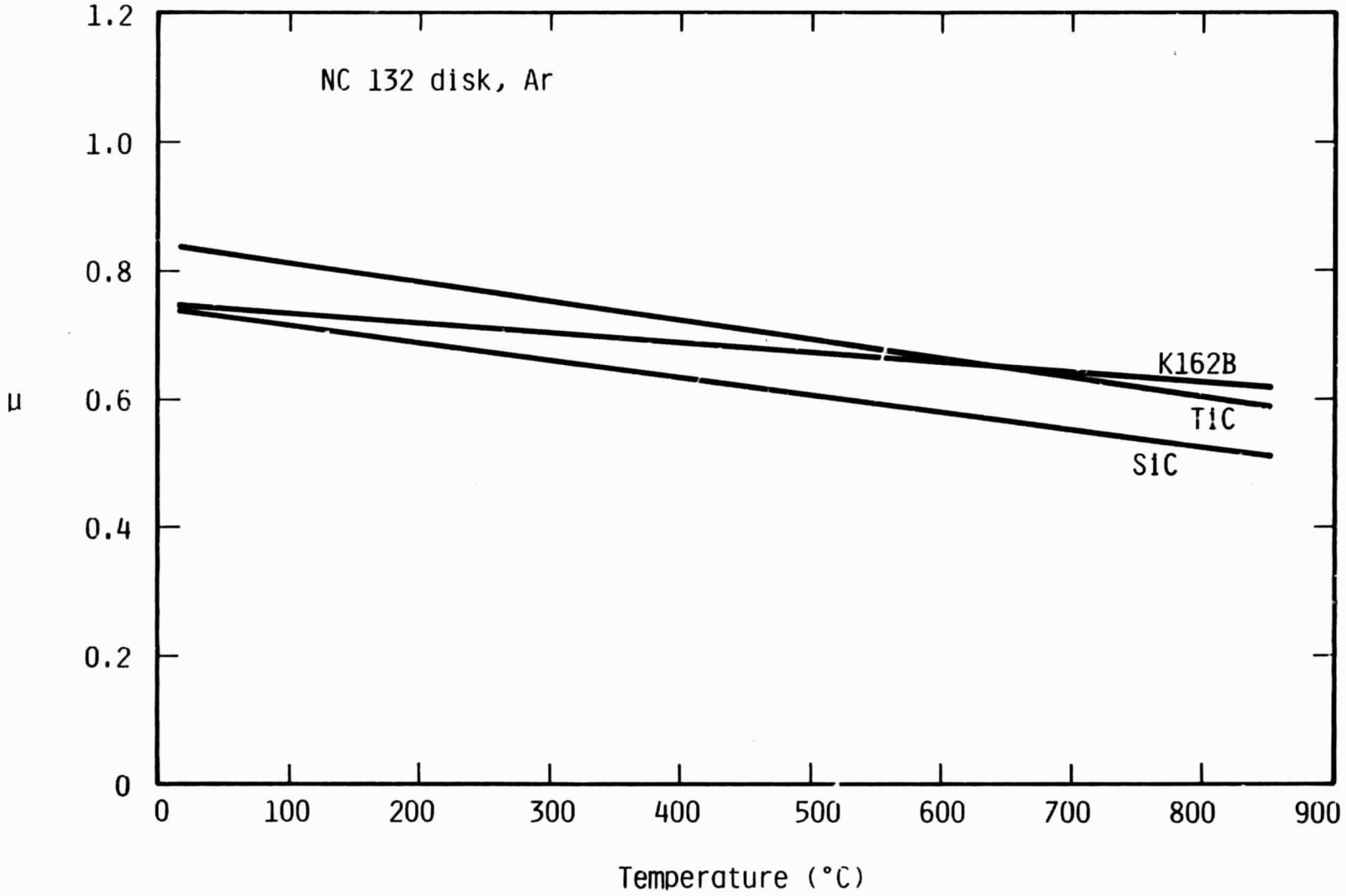

Figure 23. Friction Coefficient Versus Temperature for All Pin Materials on NC 132 Disks in Ar.

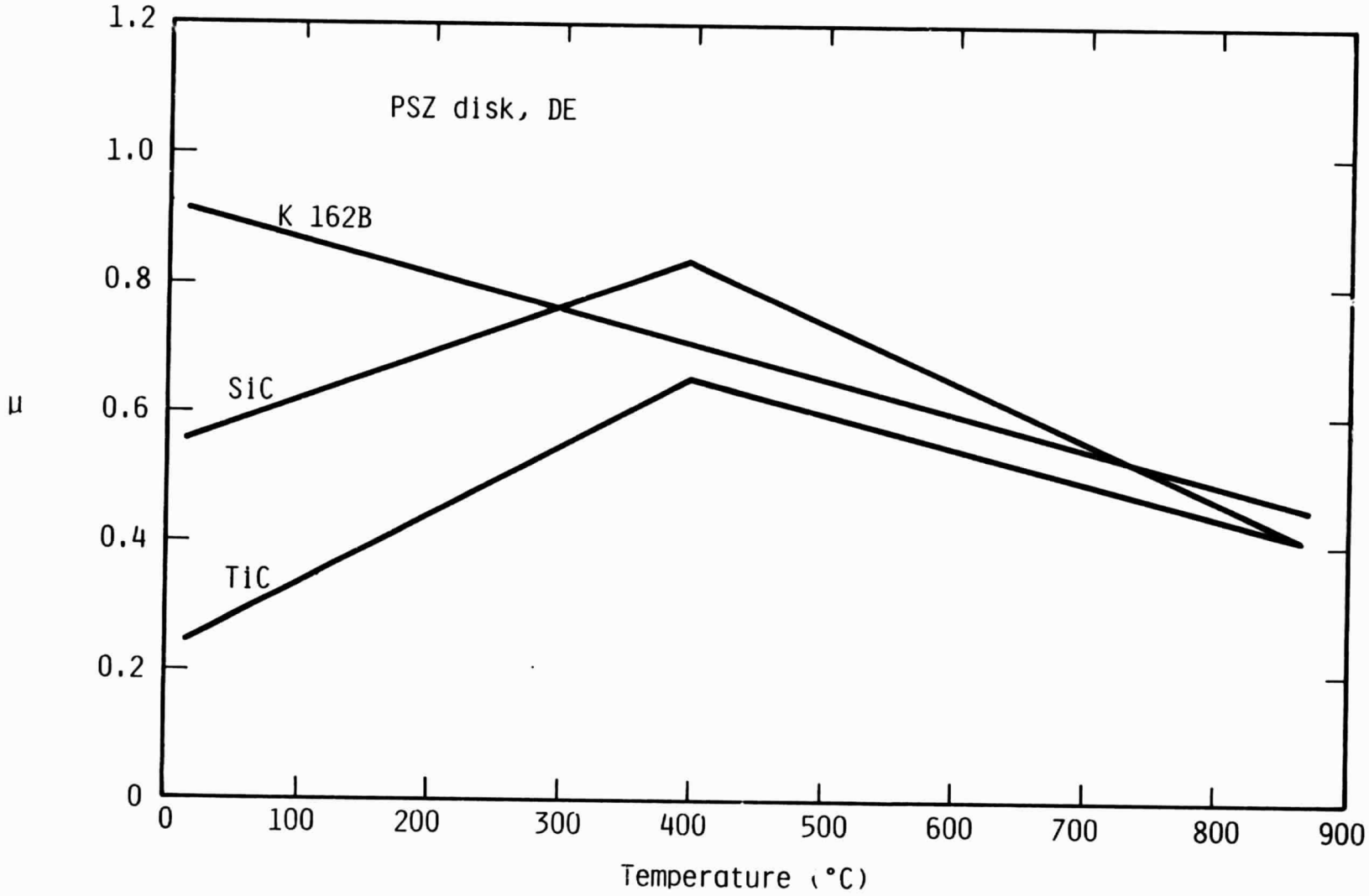

Figure 24. Friction Coefficient Versus Temperature for All Pin Materials on PSZ Disks in DE.

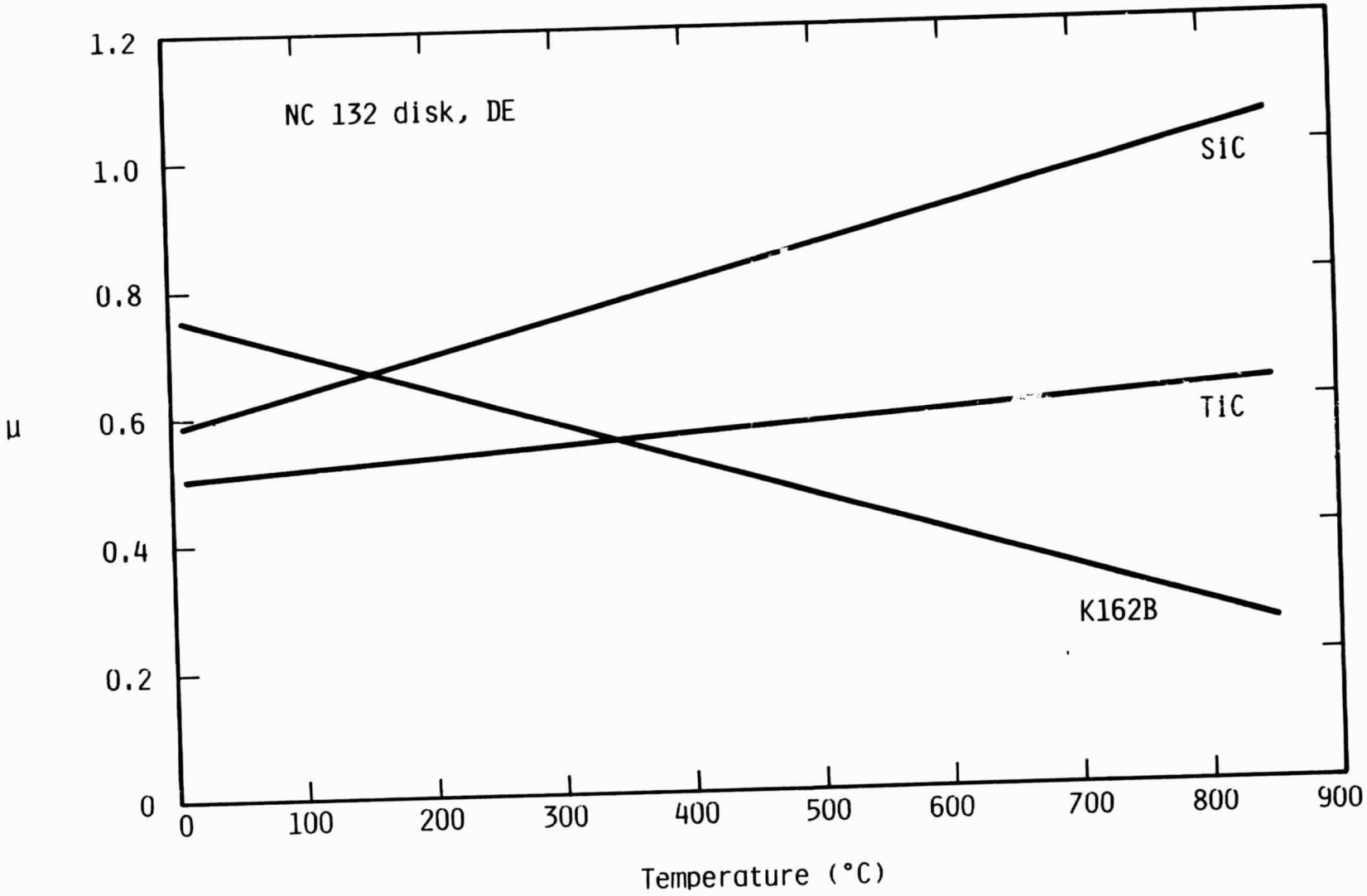

Figure 25. Friction Coefficient Versus Temperature for All Pin Materials on NC 132 Disks in DE.

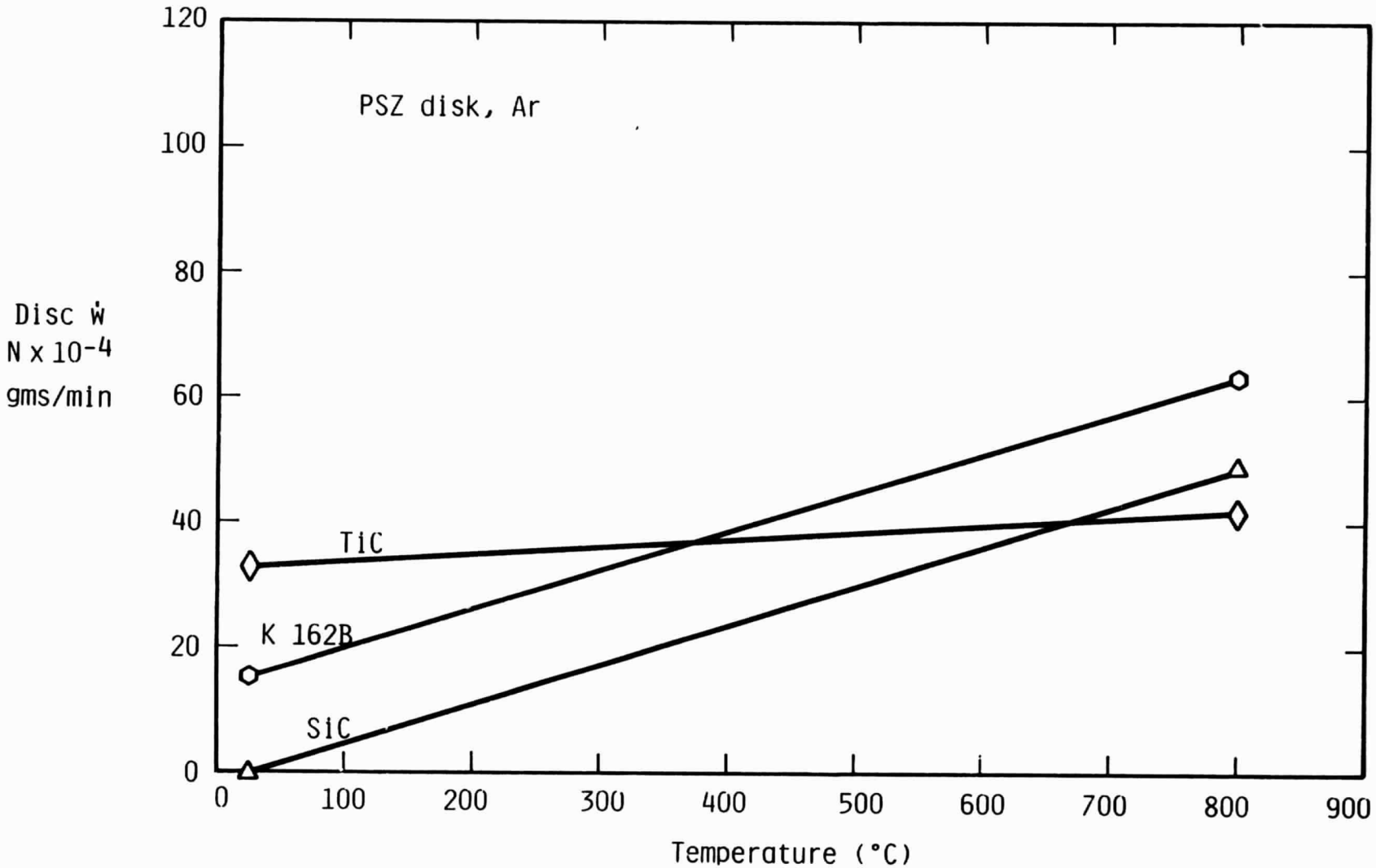

Figure 26. Wear Rate Versus Temperature for PSZ Disks in Ar.

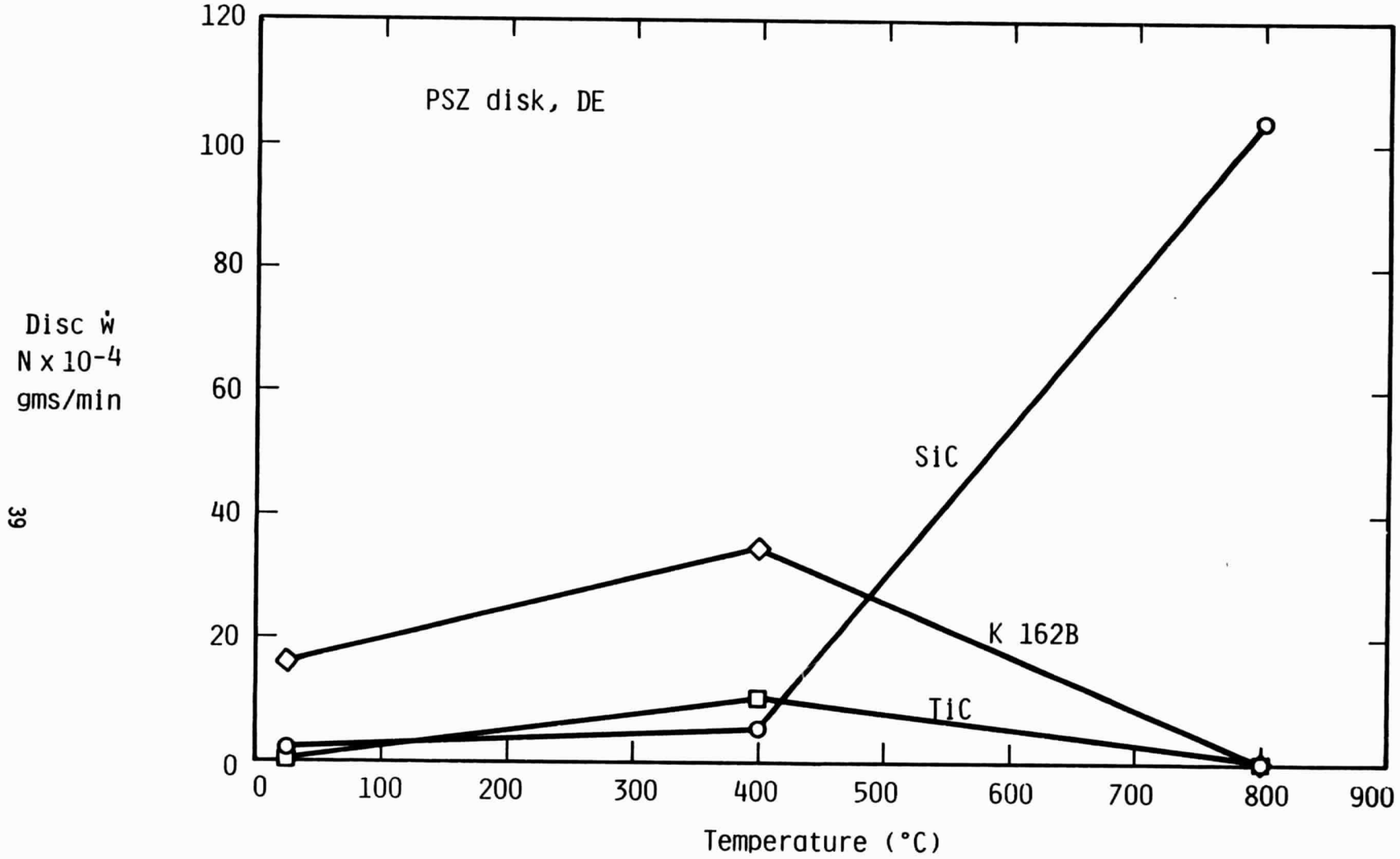

Figure 27. Wear Rate Versus Temperature for PSZ Disks in DE.

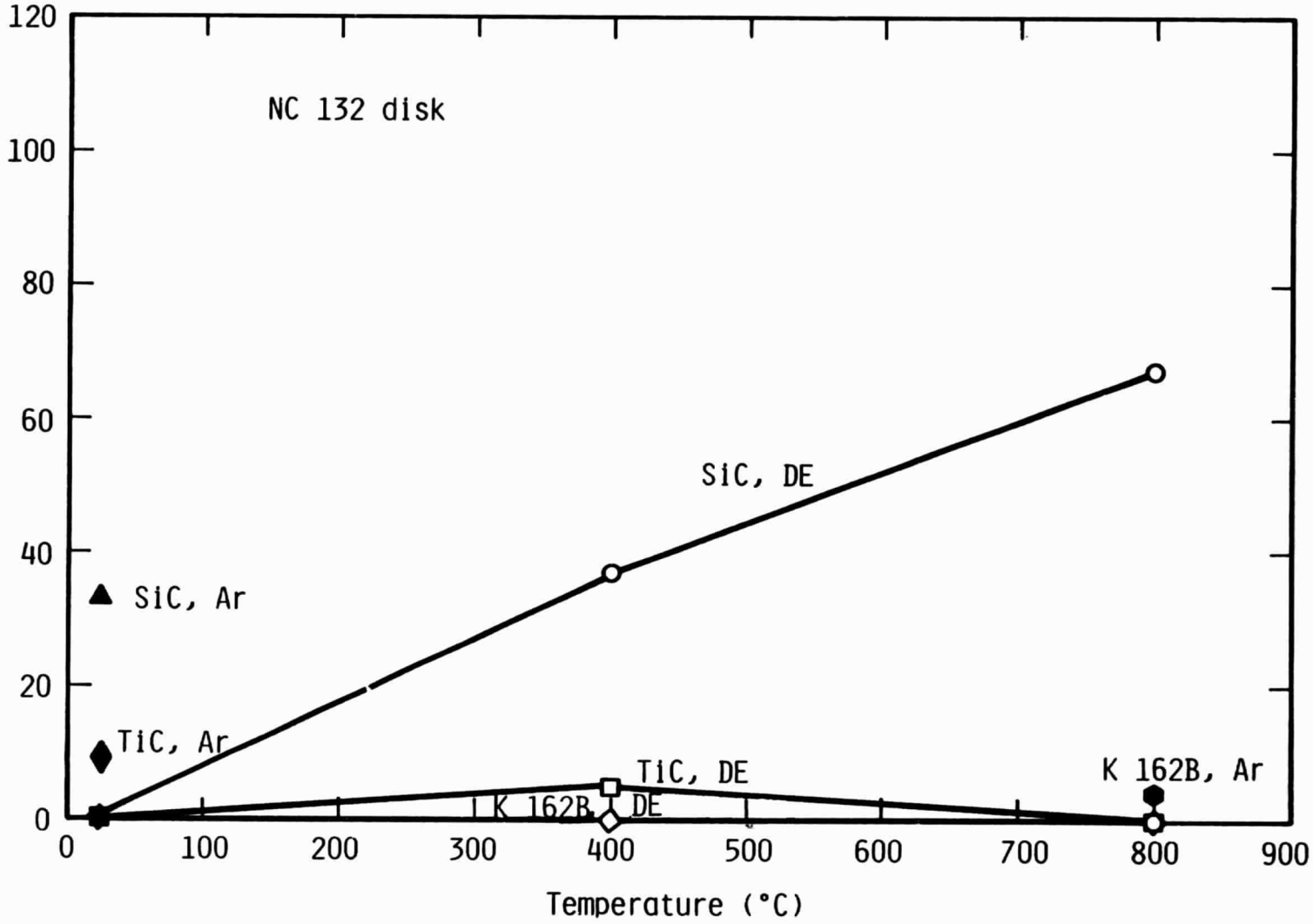

Figure 28. Wear Rate Versus Temperature for NC 132 Disks in DE and Ar.

3. Wear Characterization

Somewhat surprisingly, wear via cone and/or radial crack formation was not the most commonly observed mode of damage. In fact, it was observed clearly in only one instance, i.e., for SiC pins sliding on an NC 132 disk at 23°C in DE. As shown in Figure 29 (b and c), the cracks penetrate at a fairly steep angle, and interact to form irregularly-shaped chips (wear particles). The NC 132 disk on the other hand, manifests the much more commonly observed wear mechanism of delamination, the early stages of which, associated with the edges of plastic wear tracks, are shown in Figure 29a. Examples of such wear, during later stages, are shown in Figure 30 for NC 132 and PSZ disks.

The development of delamination in PSZ disks due to SiC pins can be seen in Figure 31, which shows several aspects of the process. In Figure 31a, delaminates (arrows) have formed after no more than a few passes. Close study of equilibrium wear regions (Figure 31b) shows that they are composed of thin sheets in the process of being removed (Figure 31c) surrounded by delaminated zones (Figure 31d) which once held material, and now consist of depressed regions containing fine wear particles. Delaminated sheets of PSZ can be found lying here and there on the disk (Figure 32), on the SiC pins (Figure 33a), and within pores in the SiC (Figure 33b); energy dispersive X-ray spectroscopy was used to identify the latter.

It is interesting to observe the inverse influence of PSZ disks upon SiC pins. Figures 34a and 34b show views of unworn and worn sectors of a pin; Figures 34c and 34d show similar views at higher magnification. Generally, since most of the materials studied are insulators, SEM specimens were coated with palladium in order to prevent charging. In the present instance, the specimen is not coated, since it is a semiconductor. Nevertheless, certain segments are glowing (charging), indicating that they are PSZ particles or sheets transferred to the pins (The SiC specimen in Figure 33 was coated.). Further, extensive plastic deformation of the SiC is evident in Figure 34d. This is somewhat surprising, since the hardness of PSZ under these conditions (23°C, DE) is about 10.5 GPa, while that of SiC is approximately 31.0 GPa, almost three times higher.

This plastic deformation has a profound effect on the wear of the SiC, as seen in Figure 35. In the first stage of wear (Figure 35a), plastic flow outlines certain carbides. As wear proceeds, adjoining particles are placed in higher relief (Figure 35b) by the plastic flow process, and eventually pits (Figure 35c) are eroded around the carbides. Finally, the particles are fully exposed (Figure 35d); their subsequent removal is a major component of pin weight loss.

At times it was observed that similar features had distinctly dissimilar origins. Figure 36, for example, shows pin and disk wear surfaces for K162 pins run on NC 132 disks at 23°C in DE. The equilibrium pin wear surface (Figure 36a) wore via delamination, and was covered with

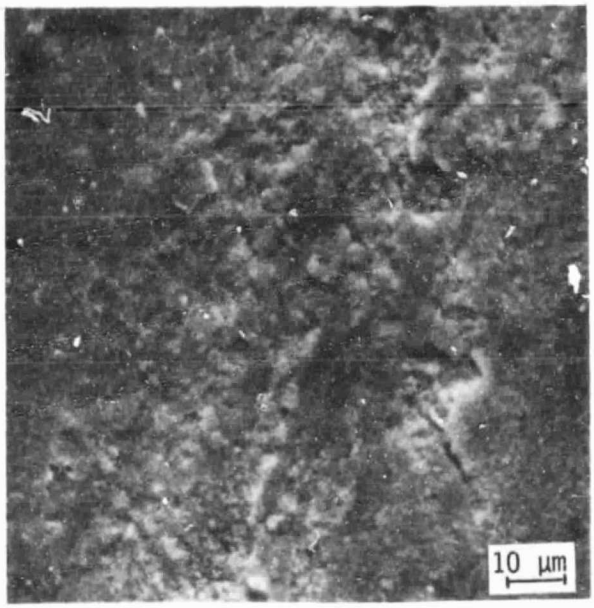

(a) Early wear, NC 132 disk

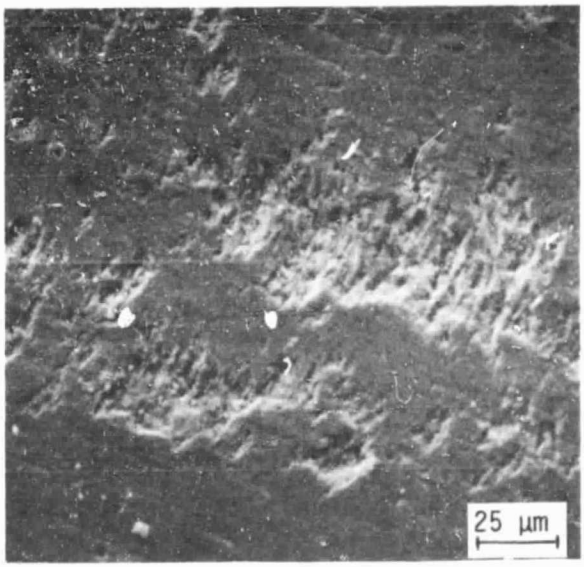

(b) Initial wear, SiC pin

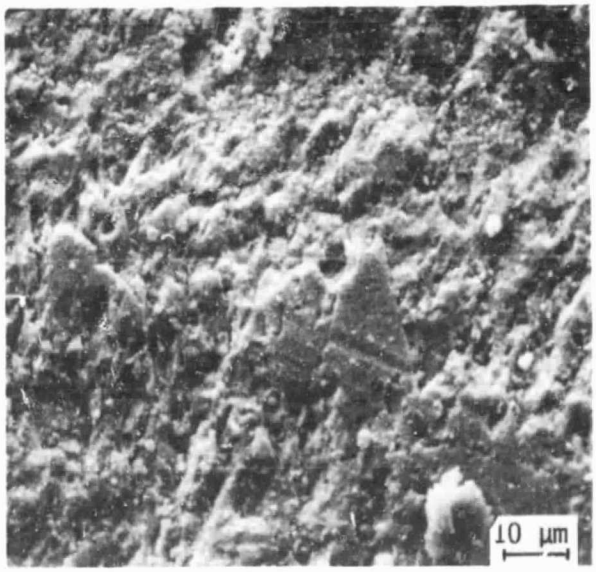

(c) Equilibrium wear, SiC pin

Figure 29. SiC Pin/NC 132 Disk, 23°C in DE, Showing Early Stage of Delamination in NC 132 Disk, and Radial or Cone-Crack Wear Particle Formation in SiC pins.

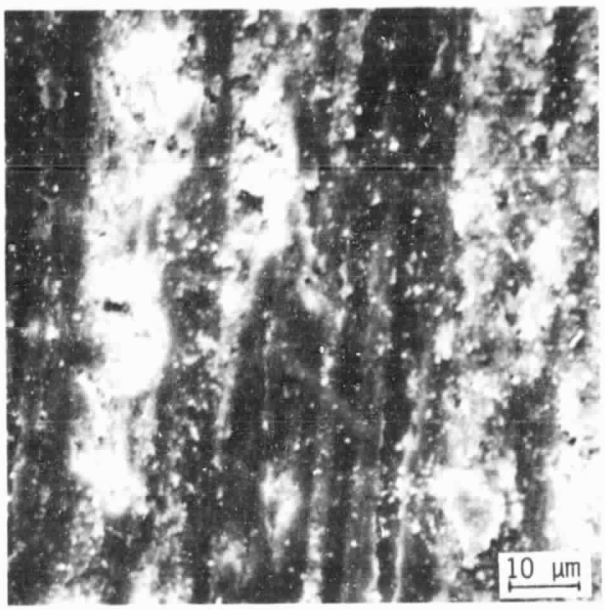

(a) NC 132 disk (SiC pins)

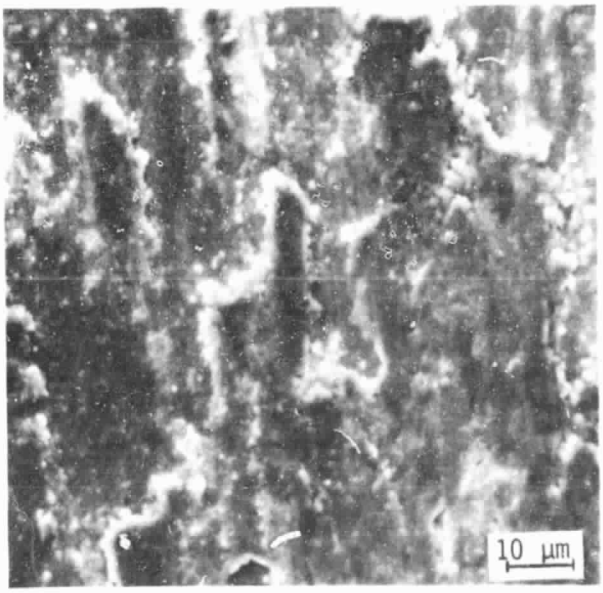

(b) PSZ disk (SiC pins)

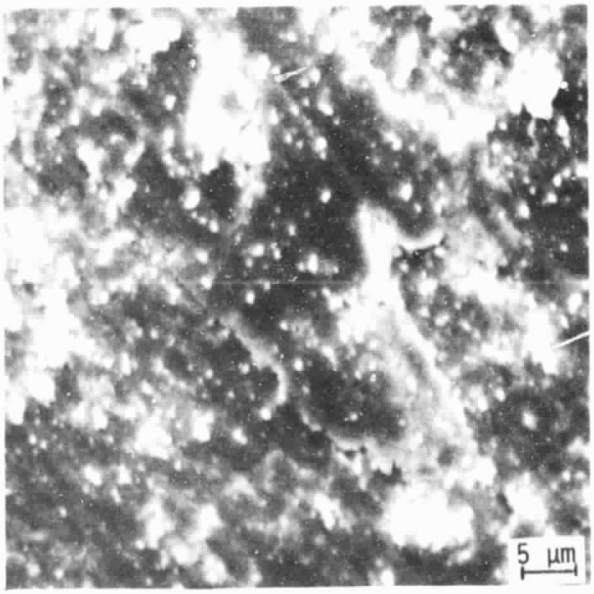

(c) PSZ disk (TiC pins)

Figure 30. Examples of Delamination in NC 132 and PSZ Disks During Equilibrium Stage of Wear, 23°C in DE.

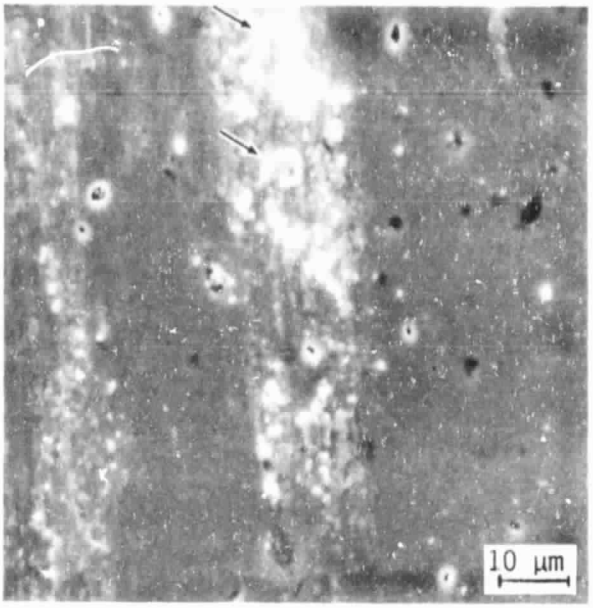

(a) Early damage, disk; arrows indicate delamination

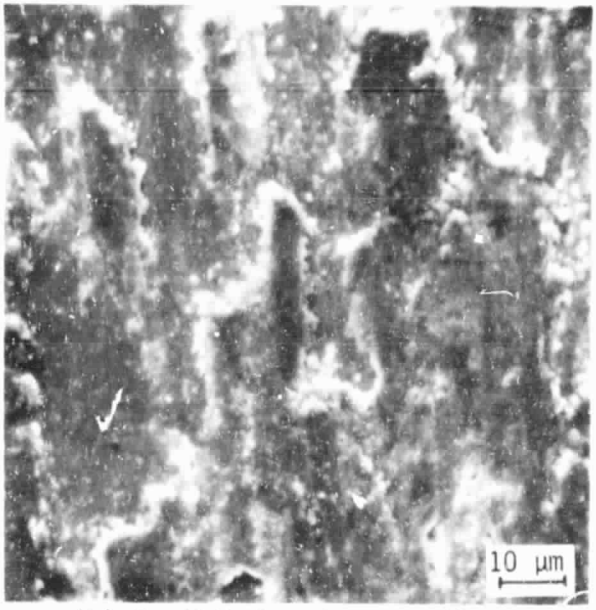

(b) Equilibrium damage, disk

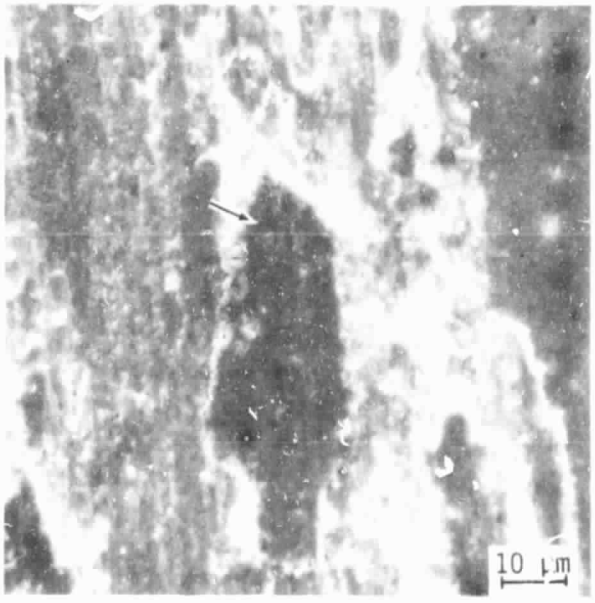

(c) Thin sheet (arrow) in process of delamination, disk

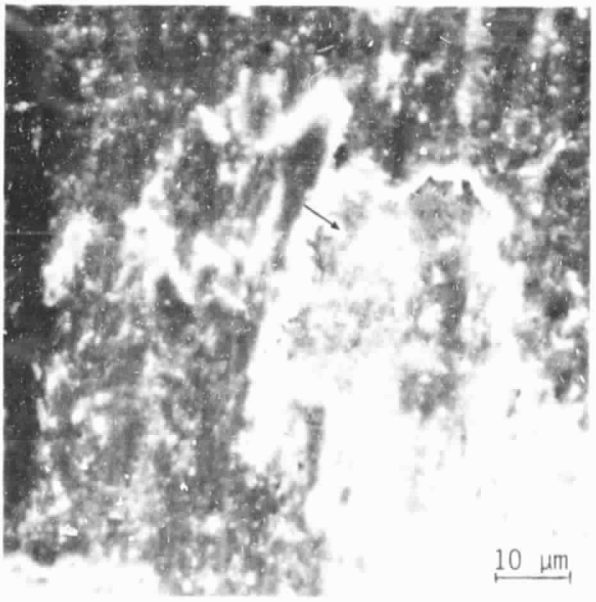

(d) Delaminated zone (arrow), disk

Figure 31. Delamination Development in PSZ Disks During Sliding of SiC Pins at 23°C in DE.

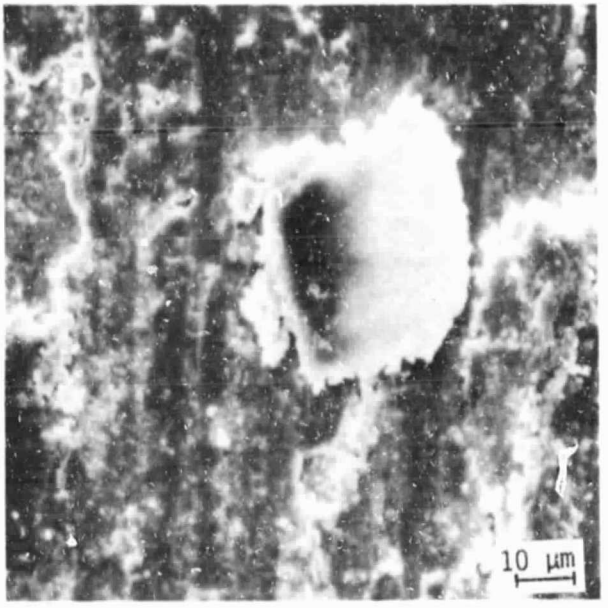

(a) Delaminated sheet on disk

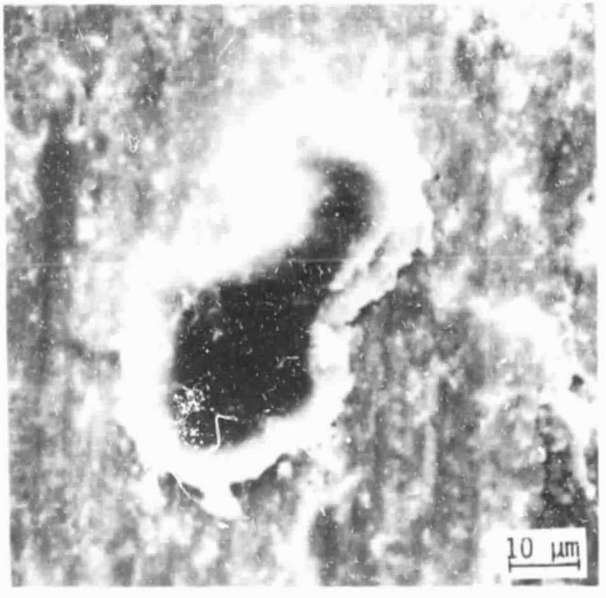

(b) Delaminated sheet on disk

Figure 32. PSZ Delaminate Sheets Lying on the Surface of the PSZ Disk; SiC Pins at 23°C in DE.

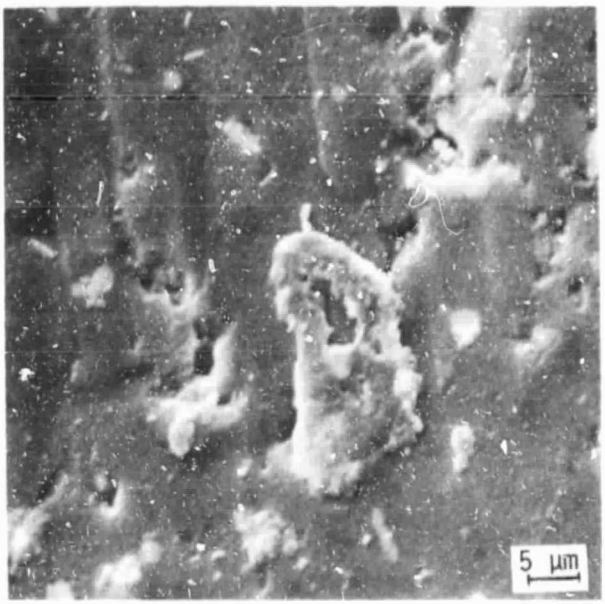

(a) PSZ delaminated sheet on SiC pin

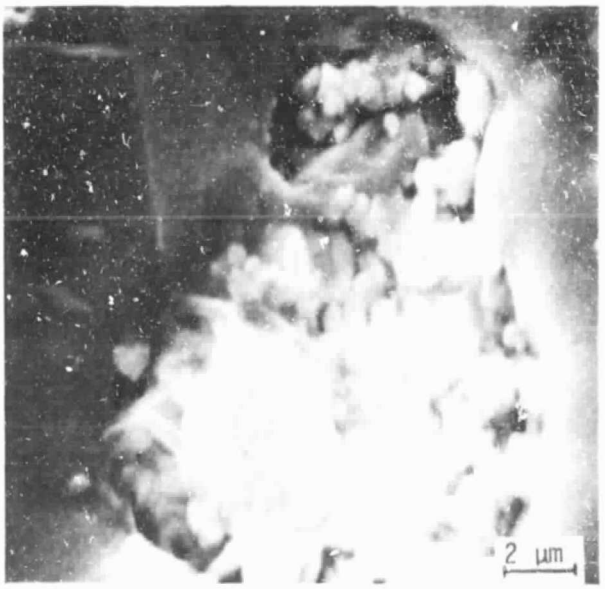

(b) Deposit within pore in SiC pin

Figure 33. PSZ Deposited onto SiC Pins at 23°C in DE.

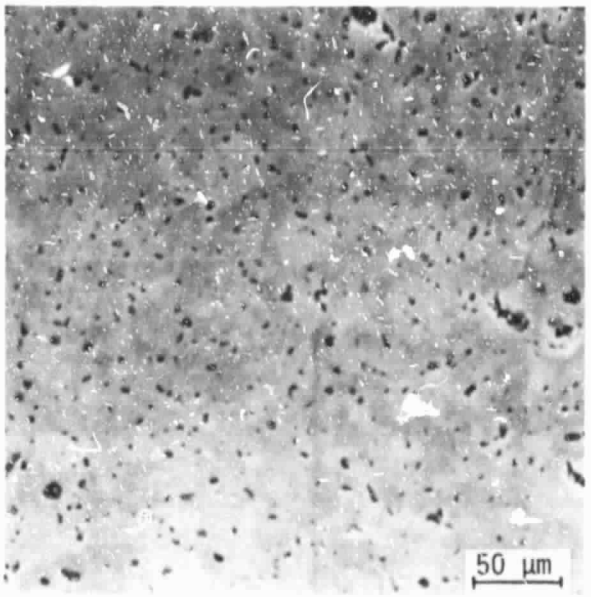

(a) Unworn pin, uncoated

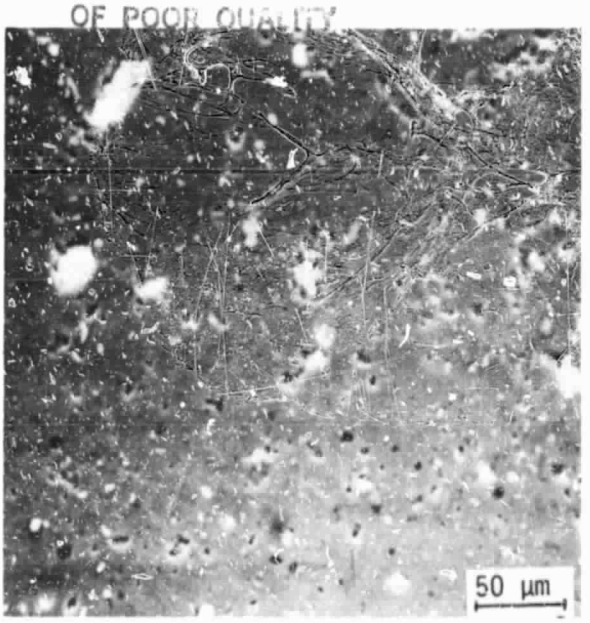

(b) Early wear pin, uncoated

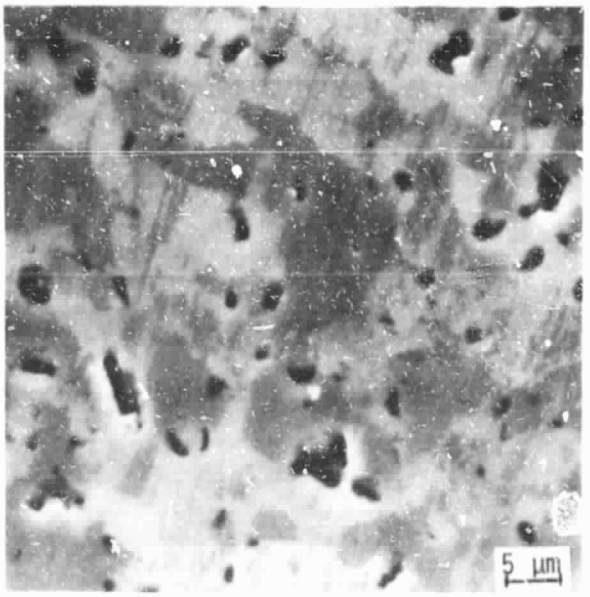

(c) Unworn pin, uncoated

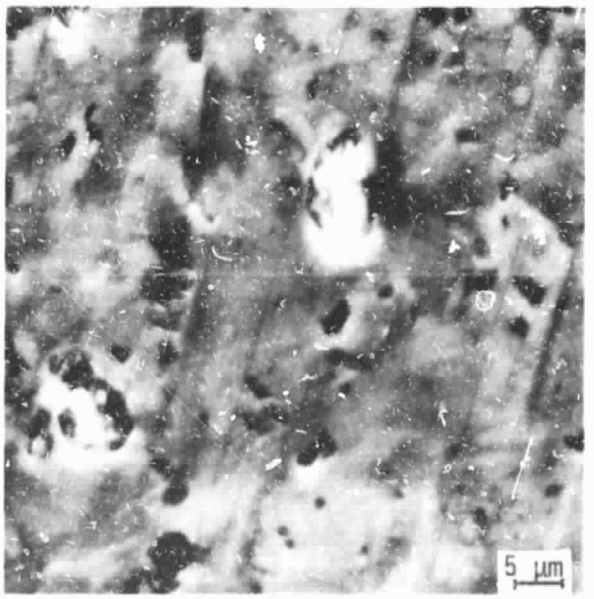

(d) Moderate wear pin, uncoated

Figure 34. Transfer of PSZ Disk Material to, and Plastic Deformation of, SiC Pin Material.

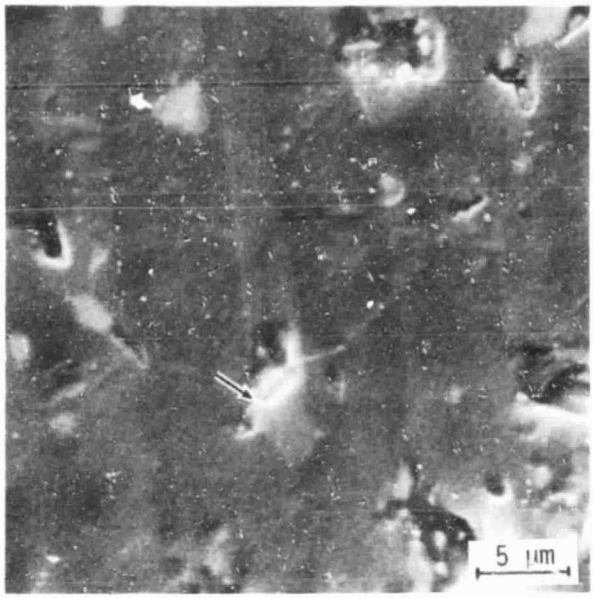

(a) Early wear, carbides come into relief (arrow) due to plastic flow in surrounding matrix

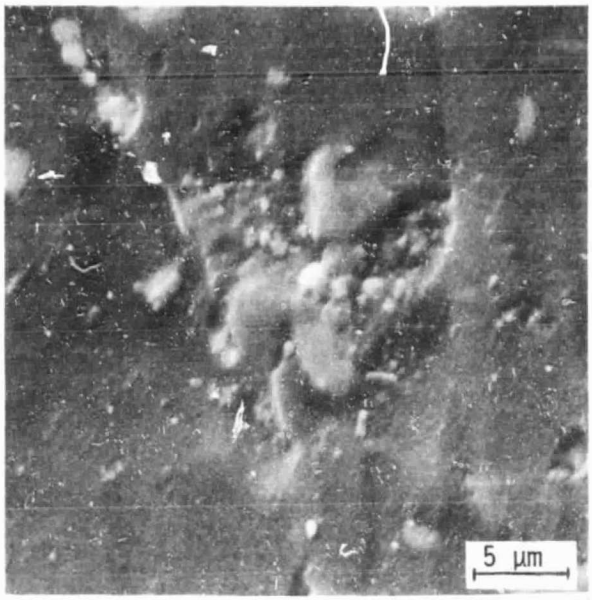

(b) Later wear, particle relief

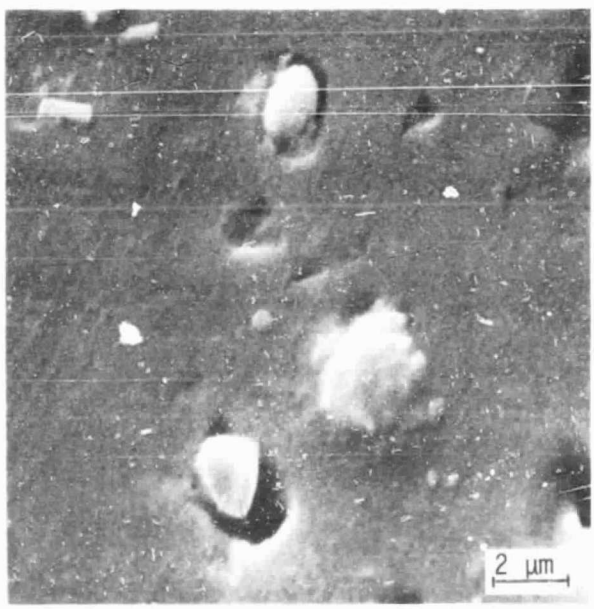

(c) Later wear, erosion of pits around particles

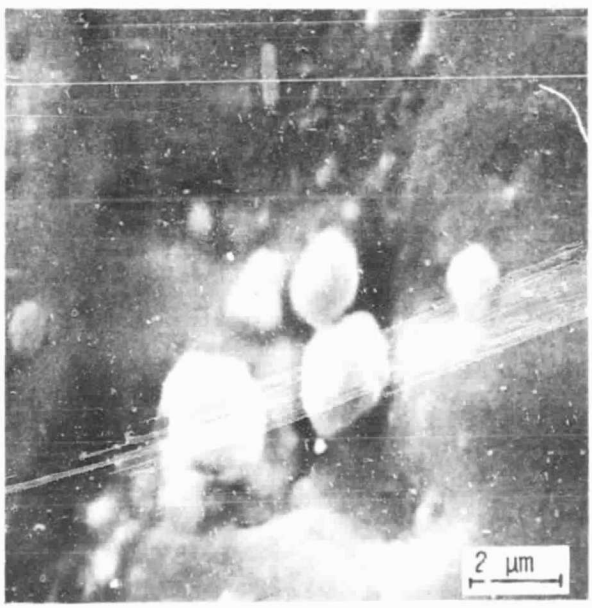

(d) Final wear, particles fully exposed

Figure 35. SiC Pin Wear Due to Plastic Deformation Induced by a PSZ Disk, 23°C, DE.

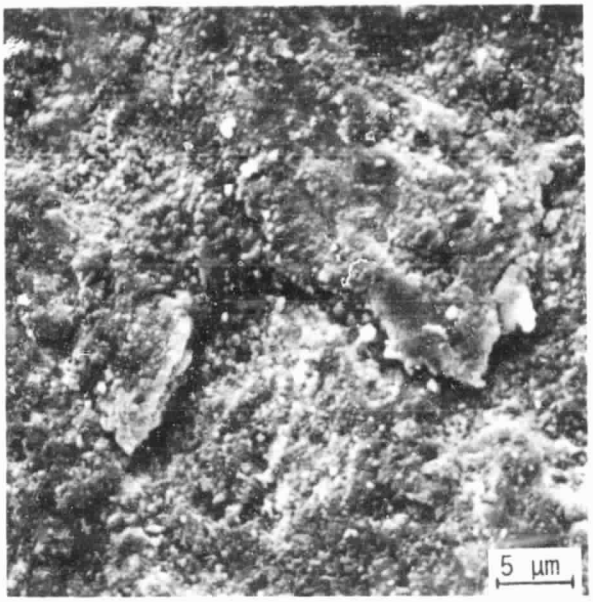

(a) Equilibrium wear, pin

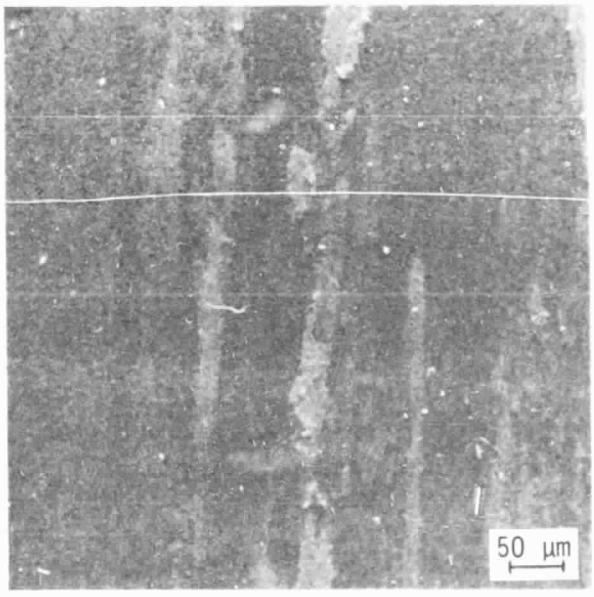

(b) NiMoX deposit, disk

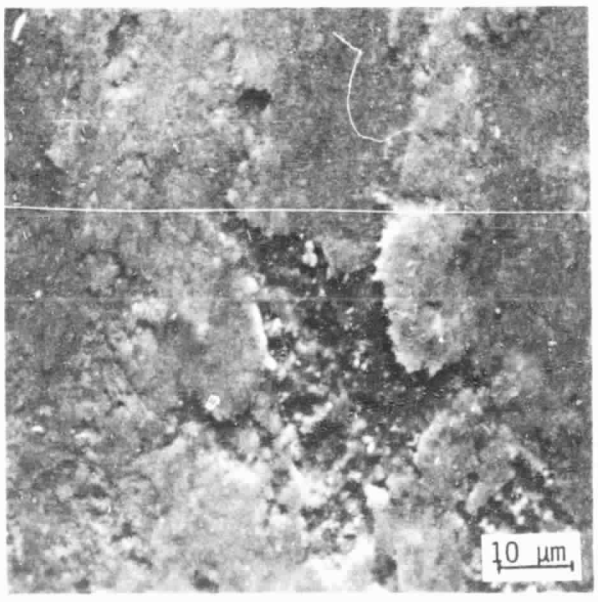

(c) Delamination of NiMoX deposit, disk

Figure 36. Wear of K162 Pins/NC 132 Disk in DE at 23°C.

particulate debris; no evidence of plastic scoring was observed. The corresponding disk surface (Figure 36b) exhibited very low wear, and had a transfer coating composed of Ni, Mo (energy dispersive spectroscopy), and possibly oxygen*. As shown in Figure 36c, this coating itself experienced delamination.

Figure 37 shows a nominally similar case; only the environment has been altered, to Ar. In this case, the pin still delaminates, but the laminae exhibit plastic scoring (Figure 37a), and are relatively smooth. No debris particles are present. The disk wear track (which is basically not worn at all) is composed of a NiMo coating (Figure 37b), and probably little or no oxygen, since the environment was inert. Nevertheless, this coating was also delaminated in sheets (Figure 37c), like the preceding was formed in DE. The ductility of the Ar-environment coating is evident in its flexure adjacent to the delaminated region.

K162B was not the only pin material which produced disk transfer layers. In particular, TiC pins run against NC 132 and PSZ disks produced layers tentatively (based on EDS, pending AES) identified as TiO_2. Due to the lubricating qualities of these deposits, which were formed at all temperatures (Figure 38), disk wear was minimal. The TiO_2 deposit appeared much more brittle and fragile than the NiMo-based K162B coatings discussed previously.

It appears that Ni and Mo can transfer from K162B whether or not oxygen is present. Figure 39 shows a K162B pin following wear against an NC 132 disk at 800°C in Ar. As shown in Figure 39a, the transition wear region is quite complex, the earliest stages of damage denoted by A, and equilibrium wear by B. Figures 39b and 39c show higher magnification views of these respective regions. Region A seems to consist of laminate sheets in the early stages of formation, while Region B is a plastically scored, delaminated area. The effect of this surface degradation upon a mating NC 132 disk is shown in Figure 40, in which a rather coarse textured coating of NiMo has been formed.

The preceding situation contrasts remarkably with that which prevails upon changing the environment from Ar to DE. In this case, the transition region (Figure 41a) is even more complex than for Ar. The early (A) and equilibrium (B) sectors border a band in which the lath-like TiC particles have been completely exposed by selective removal of the surrounding NiMo matrix. During the initial stages of wear (Figure 41b), the TiC particles can be seen gradually coming into view, lying in between matrix regions which have an etched appearance. The equilibrium wear surface (Figure 41c) displays worn or broken TiC particles lying on a rough etched background; there is no evidence of delamination. The mating disk surface (Figure 41d) is totally unworn, and covered with small, smooth, apparently loosely adherent, particles. There is no continuous surface film, as in numerous other instances involving K162B pins. It should be recalled that this last case exhibited absolutely no measurable wear, and the lowest measured friction coefficient, i.e., 0.24.

---

*Pending Auger spectroscopic analysis.

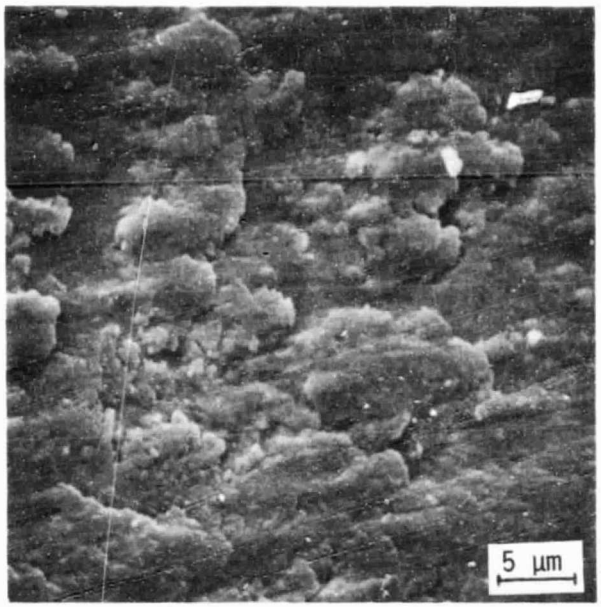

(a) Equilibrium wear, pin

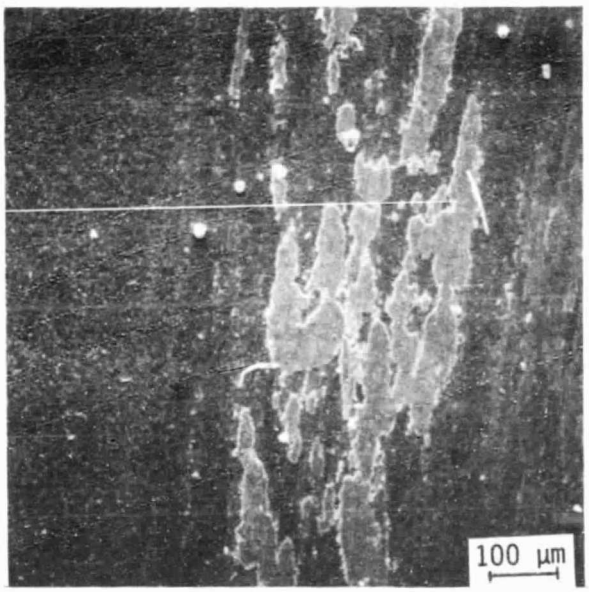

(b) NiMo deposit, disk

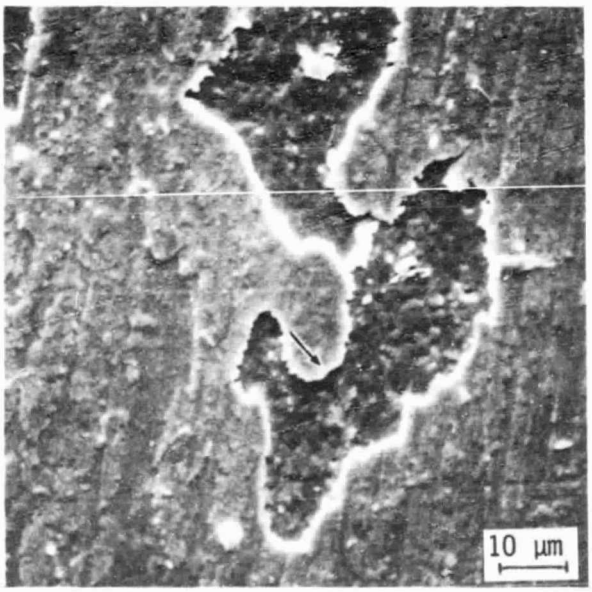

(c) Delamination NiMo deposit, disk
Flexure (arrow) of the coating
is evident

Figure 37. Wear of K162B Pins/NC 132 Disk in Ar at 23°C.

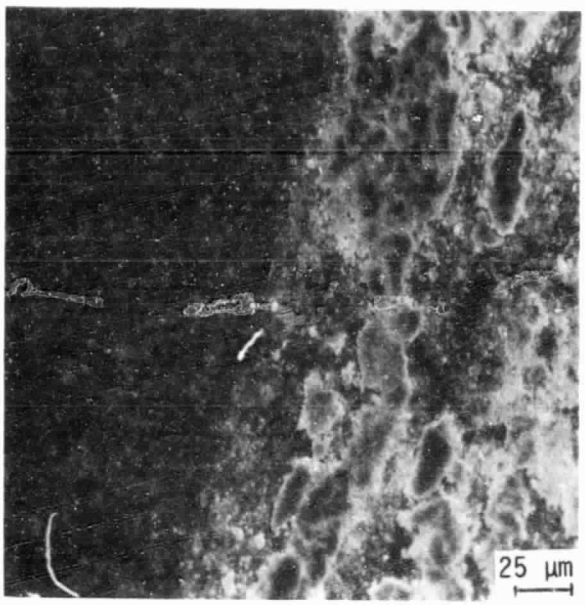

(a) TiO_2 deposit, disk, 23°C

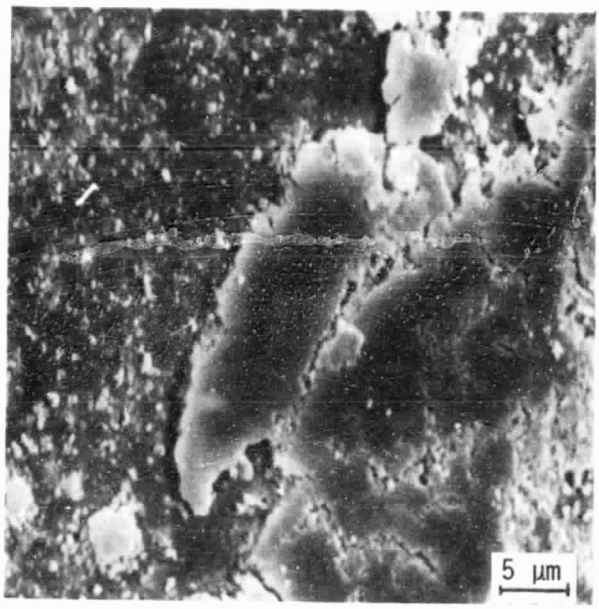

(b) Details TiO_2 deposit, disk, 23°C

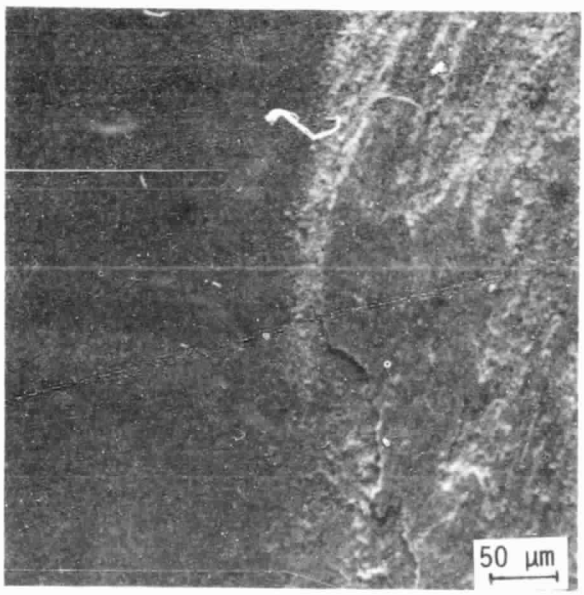

(c) TiO_2 deposit, disk, 800°C

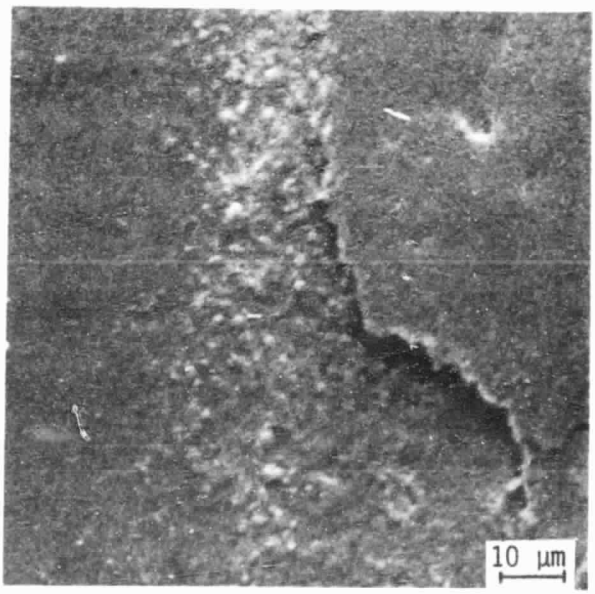

(d) Details TiO_2 deposit, disk, 800°C

Figure 38. TiO_2 Deposits on NC 132 Disks Run Against TiC Pins in DE.

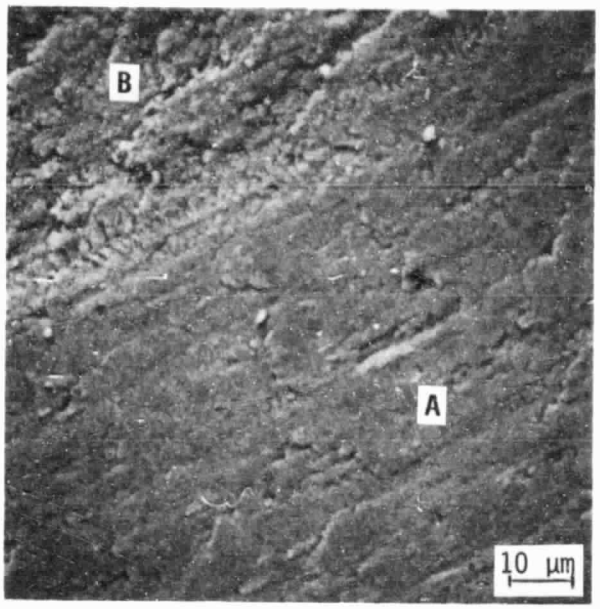

(a) Transition wear

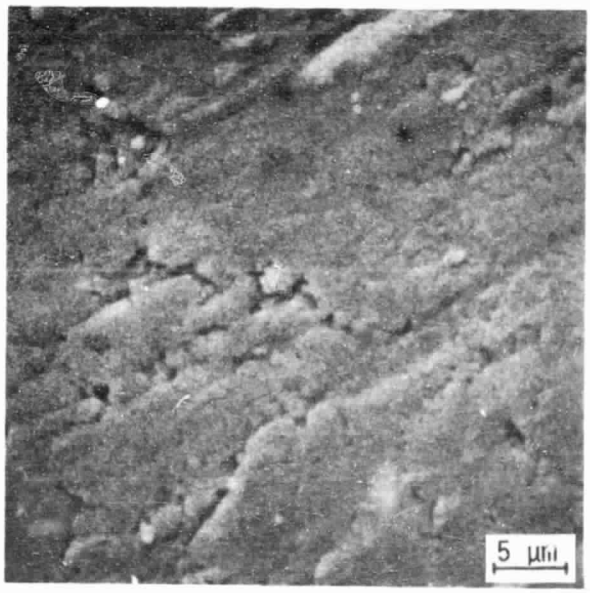

(b) Initial wear, Region A

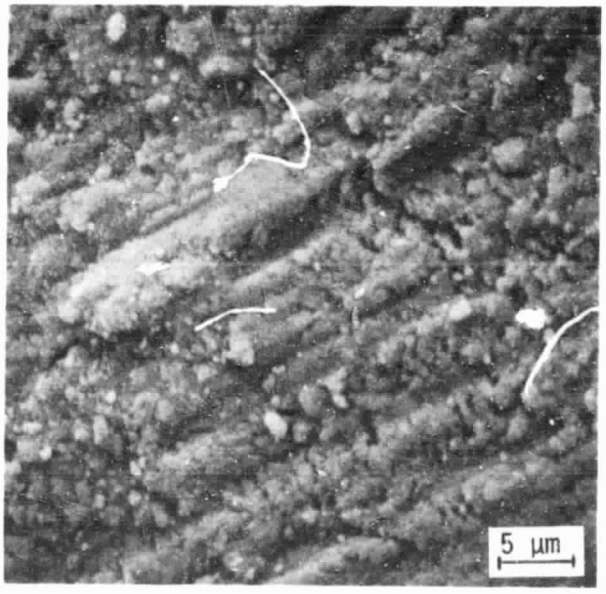

(c) Equilibrium wear, Region B

Figure 39. K162B Pin, After Wear Test Against NC 132 Disk at 800°C in Ar.

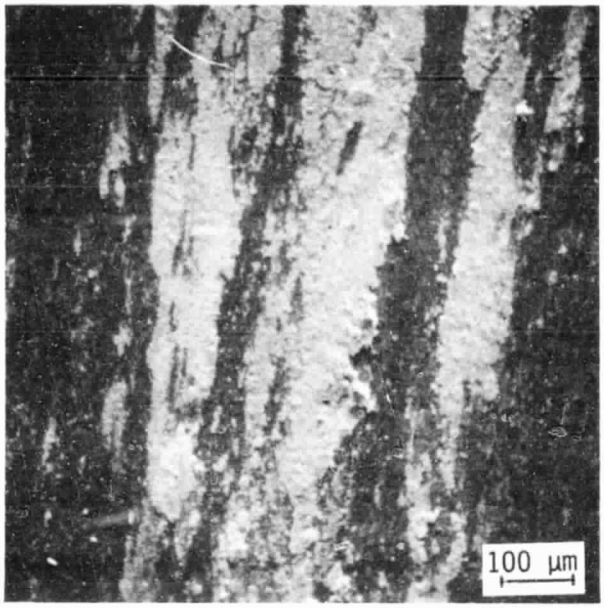

(a) NiMo deposit

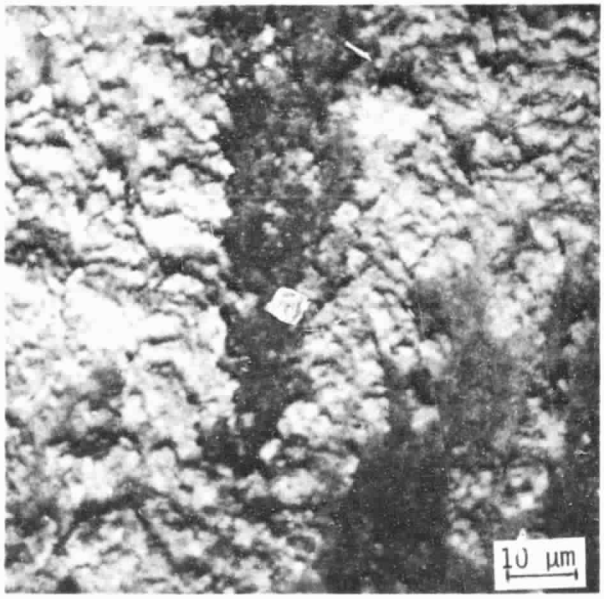

(b) Microstructure NiMo deposit

Figure 40. NC 132 Wear Track, After Wear Test Against K162B Pins at 800°C in Ar.

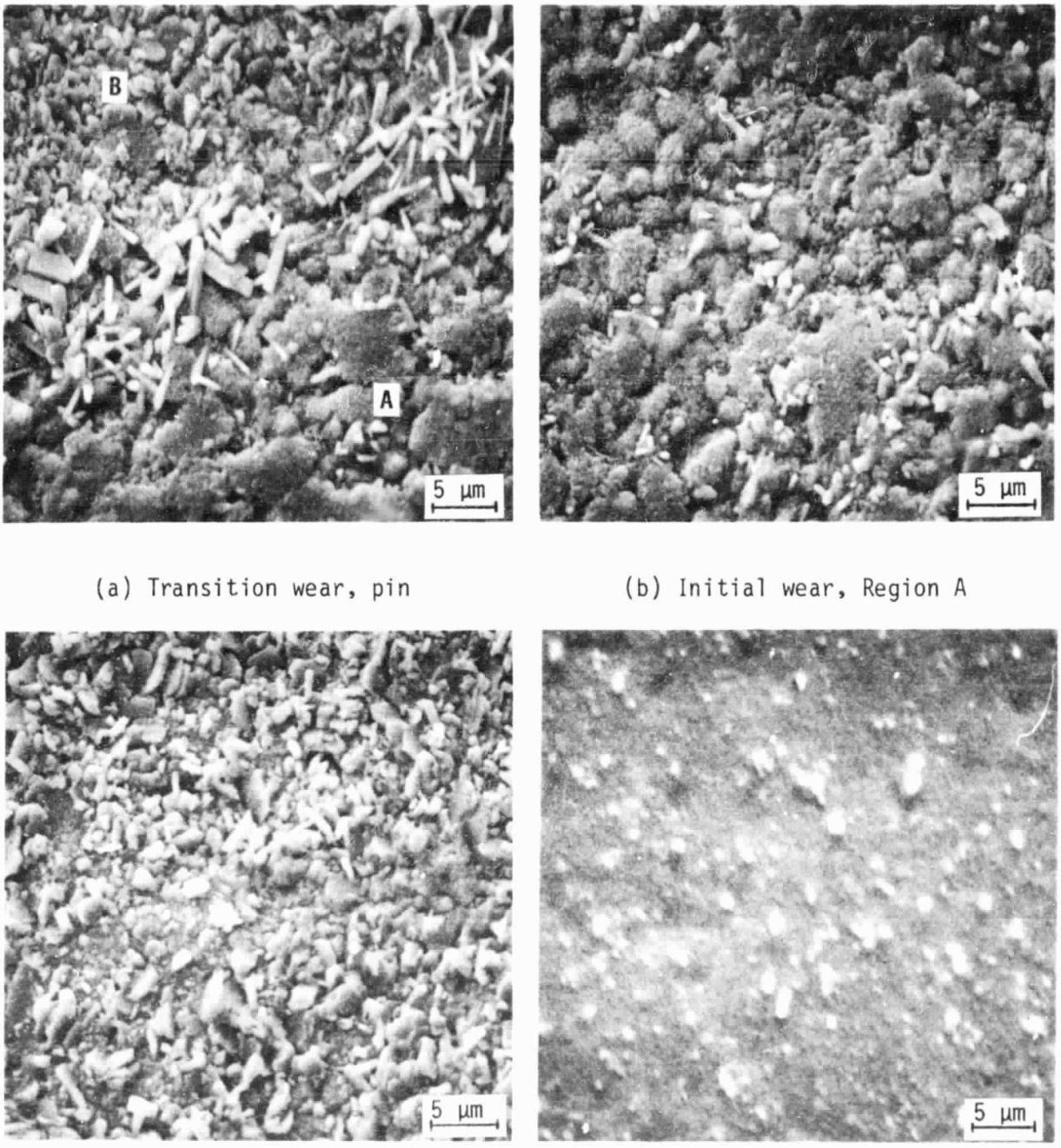

(a) Transition wear, pin

(b) Initial wear, Region A

(c) Equilibrium wear, Region B

(d) Disk wear surface

Figure 41. K162 Pin/NC 132 Disk Wear Surfaces After Testing at 800°C in DE.

Similar results were observed for K162B pins run against PSZ, although characterization of the transfer products is presently incomplete. It also was observed that at elevated temperature in high wear situations, especially with SiC pins, there was a tendency for the color of the wear track to change from cream to light yellow. The potential significance of this will be discussed in the following section.

IV. DISCUSSION

The friction and wear behavior of the ceramic couples which were tested reflected the important roles of environment and temperature, and the negligible influence of electrical potential. Subsequent discussion will deal with the former.

Although the friction coefficients of all of the couples exceeded 0.2, there were encouraging results regarding wear resistance. For those cases in which TiC or K162B material was transferred to disks in the form of films, disk wear was essentially non-existent (unmeasurable via surface profilometry), and pin wear did not appear to be high once the initial sacrificial material transfer was accomplished. Apparently these films, which can form from nominal room temperature to 800°C, are lubricious, in terms of wear. Presently, however, there is no information regarding their stability for run times in excess of about one hour.

The other minimum wear case involved K162B/NC 132 at 800°C in DE, in which the transfer product consisted of small particles (Figure 41d). Evidently these particles served as microbearings, preventing intimate pin/disk contact, and thereby inhibiting wear.

It appears that the Ti from the hot pressed TiC pin material was transferred to disks via oxidation, to form TiO_2 films. However, the mechanism(s) by which the NiMo films in Ar, and the NiMoX films in DE, were transferred from K162B pins to Si_3N_4 and PSZ disks is not clear. From the appearance of the pin early wear regions in Figure 41b, it appears that NiMo may actually vaporize, and then quickly condense onto the adjacent cooler disk. One fact which is clear is that oxidation is not the only transfer mechanism, since NiMo films were observed to form in Ar, and at temperatures which would have driven off adsorbed moisture.

When disk (and heavy pin) wear was observed, it usually was in the form of delamination. This is a form of adhesive wear, in which intermittent contact nucleates shallow subsurface cracks which eventually grow to the surface, creating a thin delaminated sheet of material. This is similar to delamination which has been observed (29) in metals, and modeled based on a theory (30,31) of cyclic crack growth. However, in the present case, delaminate sheets often form within only a few, possibly even one pass. This is just as observed by Yamamoto and Buckley (32) for 304 stainless steel wear sheets produced by sliding against Al_2O_3. In fact, the photomicrographs of wear layers in the steel alloy studied by the latter look almost identical to those shown (Figure 30) for the present ceramics. Prevention of this process must involve either 1) providing sufficient lubrication to inhibit ceramic/ceramic-adhesion, and/or 2) increasing the near surface crack growth resistance of the delaminating material.

It is interesting to note that this process seems to involve the nucleation and growth of cracks which are, for at least part of their lives, totally isolated from the wear environment, i.e., they are growing in a vacuum. This suggests that the relevant strength parameter must be the fracture toughness in an inert environment such as Ar. One recalls, for example, that K_c for NC 132 was much higher in Ar than in DE at all temperatures (Figure 11), while for SiC, K_c was generally lower in Ar than for DE (Figure 12).

In a number of instances, materials which were softer (based on microhardness tests) plastically deformed nominally harder ceramics. Generally this involved PSZ disk material scoring SiC or TiC pins. This may be related to the fact that any given spot on the PSZ wear track experiences only intermittent (cyclic) abrasion, while the pins are continuously abraded. Thus, there may exist a sufficient thermal differential between the pins and disk that the pins are softer than would be expected, based on the nominal test temperature.

The change in color of the PSZ disk at high temperature may be related to a significant alteration in local material properties. Schioler, et al (33) have recently shown that aging of PSZ at 1000°C causes transformation of tetragonal phase material to the monoclinic phase, which reduces the fracture toughness and strength. In the present case, the interfacial temperatures for 800°C tests may have exceeded 1000°C by a significant factor, which could explain the color change, as well as the rapid wear due to deteriorating mechanical properties relevant to delamination.

V. CONCLUSIONS

1. Under most conditions, PSZ evidences significant wear due to delamination.

2. NC 132 wears by delamination when coupled with SiC in DE.

3. Wear of PSZ/TiC couples in DE is relatively low at all temperatures, and wear of PSZ/K162B couples in DE is low at 800°C.

4. Wear of NC 132/TiC and NC 132/K162B is very low at all temperatures.

5. TiC and K162B pins produce beneficial (low wear rate) films and oxides on both PSZ and K162B disks.

6. Film/oxide formation depends on disk/pin combination, temperature, and environment.

7. Wear rates are low only when either lubricating films or (possibly) rolling element particles (K162B/NC 132, 800°C, DE) are formed.

8. Plastic scoring seems to be significant in many of the wear mechanisms, suggesting that hardness is a controlling factor; however, friction coefficients are sensitive to environment, indicating the importance of factors other than plastic scoring (hardness) in the adhesion process.

9. Friction coefficients are quite high, ranging from 0.24 (NC 132/K162B in DE at 800°C) to 1.24 (NC 132/SiC in DE at 800°C).

10. Electric potential is not influencial in modifying friction coefficients or wear rates.

11. Fracture toughness depends upon temperature and environment.

12. Depending upon the ceramic, fracture toughness in Ar may be greater than, or less than, that in DE.

13. Hardness is not very sensitive to environment, but decreases with increasing temperature for all of the ceramics.

VI. REFERENCES

1. D. J. Godfrey, Paper No. 45 in Ceramics for High Performance Applications II, J. J. Burke, E. N. Lenoe, and R. N. Katz, editors, pp. 877-892 (1978).

2. R. Kamo and W. Bryzik, SAE Paper No. 790645 (1979).

3. Anonymous, Automotive Engineering 88: 60-68 (1980).

4. Alex P. Bronwers, NASA Contractors Report No. 756, NAS3-20830 (1979).

5. D. J. Godfrey, Trans. SAE 83: 1036-1045 (1974).

6. R. Kamo, M. Woods, T. Yamada, and M. Mori, ASME Paper No. 80-DGP-14 (1980).

7. Donald H. Buckley, Ceramic Bulletin 51: 884-905 (1972).

8. Kazuhisa Miyoshi and Donald H. Buckley, Wear 77: 253-264 (1982).

9. Kazuhisa Miyoshi and Donald H. Buckley, ASLE Trans. 22: 146-153 (1979).

10. D. H. Buckley and K. Miyoshi, Wear 100: 333 (1984).

11. B. R. Lawn and A. G. Evans, J. Mat. Sci. 12: 2195 (1977).

12. A. G. Evans and D. B. Marshall, "Wear Mechanisms in Ceramics", Fundamentals of Friction and Wear of Materials, ASM, Metals Park, OH, 439 (1980).

13. M. V. Swain, Wear 35: 185 (1975).

14. B. R. Lawn, S. M. Wiederhorn, and D. E. Roberts, J. Mat. Sci. 19: 2561 (1984).

15. R. P. Steijn, Wear 7: 48-66 (1964).

16. D. J. Barnes and B. D. Powell, Wear 32: 195-202 (1975).

17. H. Shimura and Y. Tsuya, Proc. Int. Conf. Wear of Mats., St. Louis, April 1977, ASME, N.Y., 452 (1977).

18. E. F. Finkin, S. J. Calabrese, M. B. Peterson, ASLE Preprint No. 72LC-7C-2 (1972).

19. L. B. Sibley and C. M. Allen, Wear 5: 312-329 (1962).

20. Advanced Mechanical Technology, Inc., "Evaluation of Improved Materials for Stationary Diesel Engines Operating on Residual and Coal Based Fuels", U.S. Department of Energy Contract No. DE-AC-03-79ET15444 (1980).

21 D. B. Holt, Proc. Conf. on Environment-Sensitive Mechanical Behavior, Metall. Soc. (AIME) Confs., 35: 269 (1966).

22. J. H. Westbrook, Metall. Soc. (AIME) Confs., 35: 247 (1966).

23. S. A. Varchenya, G. P. Upit, and I. P. Manika, Symp. on the Science of Hardness Testing and Its Research Applications, ASM, pp. 440-444 (1973).

24. H. Shimura and Y. Tsuya, Wear 1977, ASME, pp. 452-461 (1977).

25. H. S. Shan and P. C. Pandey, Wear 32: 167-179 (1975).

26. S. N. Postnikov, Electrophysical and Electrochemical Phenomena in Friction, Cutting, and Lubrication, Van Nostrand Reinhold, New York (1978), pp. 173-212.

27. Alan West (Advanced Mechanical Technology, Inc.), personal communication (1982).

28. A. G. Evans and E. A. Charles, J. Am. Cer. Soc. 59: 371 (1976).

29. S. Jahanmir, N. P. Suh, and E. P. Abrahamson, Wear 28: 235 (1974).

30. H.-C. Sin and N. P. Suh, J. App. Mech. 51: 317 (1984).

31. N. P. Suh, Wear 25: 111 (1973).

32. Y. Yamamoto and D. H. Buckley, ASLE Trans. 26: 277 (1982).

33. L. J. Schioler, R. N. Katz, A. C. Gonzalez, and B. R. Lawn, Am. Cer. Soc. Bull. 64: 326 (1985).